Competing Effects of Elevated Vertical Mixing and Increased Freshwater Input on the Stratification and Sea Ice Cover in a Changing Arctic Ocean

PETER E. D. DAVIS,* CAMILLE LIQUE,+ AND HELEN L. JOHNSON

Department of Earth Sciences, University of Oxford, Oxford, United Kingdom

JOHN D. GUTHRIE

Polar Science Center, Applied Physics Laboratory, University of Washington, Seattle, Washington

(Manuscript received 2 September 2015, in final form 20 November 2015)

ABSTRACT

The Arctic Ocean is undergoing a period of rapid transition. Freshwater input is projected to increase, and the decline in Arctic sea ice is likely to drive periodic increases in vertical mixing during ice-free periods. Here, a 1D model of the Arctic Ocean is used to explore how these competing processes will affect the stratification, the stability of the cold halocline, and the sea ice cover at the surface. Initially, stronger shear leads to elevated vertical mixing that causes the mixed layer to warm. The change in temperature, however, is too small to affect the sea ice cover. Most importantly, in the Eurasian Basin, the elevated shear also deepens the halocline and strengthens the stratification over the Atlantic Water thermocline, reducing the vertical heat flux. After about a decade this effect dominates, and the mixed layer begins to cool. The sea ice cover can only be significantly affected if the elevated mixing is sufficient to erode the stratification barrier associated with the cold halocline. While freshwater generally dominates in the Canadian Basin (further isolating the mixed layer from the Atlantic Water layer), in the Eurasian Basin elevated shear reduces the strength of the stratification barrier, potentially allowing Atlantic Water heat to be directly entrained into the mixed layer during episodic mixing events. Therefore, although most sea ice retreat to date has occurred in the Canadian Basin, the results here suggest that, in future decades, elevated vertical mixing may play a more significant role in sea ice melt in the Eurasian Basin.

1. Introduction

The vertical structure in the Eurasian Basin of the Arctic Ocean is characterized by a cold and fresh surface mixed layer overlying a deeper warm ($T > 0$°C) and salty Atlantic Water layer (Fig. 1). The heat contained within the Atlantic Water layer is sufficient to melt all sea ice in the Arctic within a few years (Turner 2010). However, this heat is isolated from the mixed layer by the cold halocline, which is characterized by the coincidence of near-freezing temperatures with a strong salinity gradient (Fig. 1; Aagaard et al. 1981; Rudels et al. 1996; Toole et al. 2010). As salinity dominates density at low temperatures, the cold halocline creates a layer of strong stratification that limits the depth to which surface-generated mixing can penetrate, and the near-freezing temperatures ensure that any pycnocline water that is mixed up to the surface is devoid of excess heat. As a result, the only process by which the heat contained within the Atlantic Water layer can be mixed up to the surface is through diffusion, such as that associated with the breaking of internal waves or double diffusive processes.

Scattered observations throughout the Arctic Ocean have shown, however, that the energy associated with the

Denotes Open Access content.

* Current affiliation: British Antarctic Survey, Cambridge, United Kingdom.

+ Current affiliation: Ifremer, Laboratoire de Physique des Océans, UMR6523, CNRS-IFREMER-IRD-UBO, Brest, France.

Corresponding author address: Peter E. D. Davis, British Antarctic Survey, High Cross, Madingley Road, Cambridge CB3 0ET, United Kingdom.
E-mail: petvis@bas.ac.uk

DOI: 10.1175/JPO-D-15-0174.1

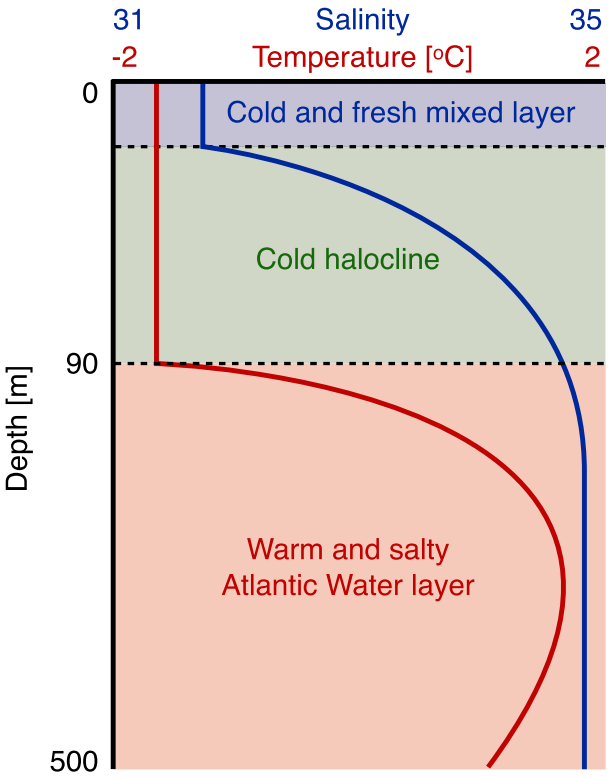

FIG. 1. Schematic of the vertical temperature (red line) and salinity (blue line) structure in the upper 500 m of the Eurasian Basin in the Arctic Ocean. The cold halocline (green layer) is characterized by the coincidence of near-freezing temperatures with a strong salinity gradient and acts to isolate the cold and fresh surface mixed layer (blue) from the heat contained within the warm and salty Atlantic Water layer (red).

internal wave field is one to two orders of magnitude smaller than that observed at lower latitudes (Levine et al. 1985, 1987; Plueddemann 1992; D'Asaro and Morison 1992; Guthrie et al. 2013). This is because of the limited generation of internal wave energy through the interaction of the barotropic tide with topography (Simmons et al. 2004; the majority of the Arctic Basin is north of the M_2 critical latitude), shielding of the ocean from direct wind forcing because of the sea ice cover (Rainville et al. 2011), and the dissipation of internal wave energy in oscillating under-ice boundary layers (Morison et al. 1985; Pinkel 2005). Consequently, the rate of vertical mixing across the cold halocline from the breaking of internal waves is only slightly larger than molecular levels, and the vertical heat flux to the surface is close to zero. For example, Shaw and Stanton (2014) show that the vertical diffusivity (K_z) in the deep central Canadian Basin averages near-molecular levels between 2.2×10^{-7} and $3.4 \times 10^{-7}\,\mathrm{m^2\,s^{-1}}$, leading to a heat flux of $0.1\,\mathrm{W\,m^{-2}}$, and Rainville and Winsor (2008) found that K_z averaged $10^{-6}\,\mathrm{m^2\,s^{-1}}$ in the deep interior basins, increasing to $10^{-5}\,\mathrm{m^2\,s^{-1}}$ in the upper ocean. In the Eurasian Basin, Fer (2009) inferred from microstructure observations that the heat flux across the cold halocline was not significantly different from zero, and Sirevaag and Fer (2012) observed a heat flux due to double diffusion of $0.6\,\mathrm{W\,m^{-2}}$. Similarly, in the Canadian Basin, Timmermans et al. (2008) observed a heat flux of 0.05–$0.3\,\mathrm{W\,m^{-2}}$. These estimates are only an order of magnitude larger than molecular diffusion alone and are significantly smaller than the value required to adversely affect the sea ice cover at the surface (Maykut and Untersteiner 1971).

The Arctic region is currently changing rapidly. Climate model projections suggest that sea ice cover at the surface will decline at such a rate that the ocean will become ice-free in summer sometime around the middle of the century (Wang and Overland 2009), and freshwater input from enhanced river runoff and positive precipitation minus evaporation ($P - E$) will increase by ≈30% by 2050 (Peterson et al. 2002; Vavrus et al. 2012; Bintanja and Selten 2014; Haine et al. 2015). Although increased freshwater input should strengthen the cold halocline by increasing the magnitude of the salinity gradient, the decline in Arctic sea ice cover may lead to periodic increases in vertical mixing through the enhancement of wind-driven near-inertial motions during ice-free periods (Pinkel 2005; Rainville and Woodgate 2009; Rainville et al. 2011). Although a substantial amount of this near-inertial energy will be lost to directly mixing the surface layer, a portion may propagate deeper where it can erode the cold halocline and enhance the vertical heat flux from the Atlantic Water layer (Fer 2014). Consequently, the interplay between enhanced freshwater input and elevated vertical mixing may play a significant role in determining how the vertical heat flux to the underside of the sea ice will change over the coming decades. As even a small change in the vertical heat flux may have irreversible impacts on sea ice cover at the surface (Maykut and Untersteiner 1971; Polyakov et al. 2012), understanding these processes is critical.

While observations already show that excess freshwater is accumulating in the Arctic Ocean (e.g., Rabe et al. 2011), it is not yet clear whether vertical mixing is increasing, despite an average decrease of 14% ± 3% $\mathrm{decade^{-1}}$ in the September sea ice extent between 1979 and 2012 (Overland and Wang 2013), and an average increase in the Arctic-wide melt season length of 6 $\mathrm{days\,decade^{-1}}$ over the same period (Markus et al. 2009). For example, the analysis of expendable current profiler (XCP) data collected in the 1980s and late 2000s by Guthrie et al. (2013) shows that there has been no temporal trend in vertical mixing over the thermocline, and the pan-Arctic microstructure measurements reported in Rippeth et al. (2015) suggest that vertical mixing

over the Atlantic Water layer thermocline shows no dependence on sea ice cover. In contrast, Rainville and Woodgate (2009) observed a dramatic increase in the strength of vertical mixing in the upper 100 m during ice-free periods in the Chukchi Sea, with the average diffusivity increasing from molecular levels during winter to $2 \times 10^{-4}\,m^2\,s^{-1}$ during summer. Similarly, Dosser et al. (2014) observed a seasonal cycle in the amplitude of wind-driven near-inertial waves in the upper 200 m of the Canadian Basin in response to the annual cycle in sea ice cover. During summer the average amplitude increased by 0.45 m over the winter value, despite the weaker winds, suggesting a strong coupling between sea ice conditions and the inertial wave field. In addition, the appearance of a second autumn phytoplankton bloom in the Arctic, which is correlated with delayed freeze-up and increased exposure of the ocean to direct wind forcing, provides indirect evidence that elevated vertical mixing is driving a supply of nutrients into the mixed layer during these periods (Ardyna et al. 2014); in the ice-free Chukchi Sea, Nishino et al. (2015) also observed a peak in nutrient fluxes and primary productivity associated with gale force winds and enhanced turbulent mixing (Kawaguchi et al. 2015).

Despite the lack of a consistent pan-Arctic signal, which might still be too small to detect, the decline in Arctic sea ice cover is very likely to result in periodic increases in vertical mixing during ice-free periods, as the ocean is more easily forced by the winds (Tsamados et al. 2014; Martin et al. 2014), and the magnitude of under-ice dissipation is reduced. The aim of this paper is to explore how the competing effects of elevated vertical mixing and freshwater input will affect the stratification, the stability of the cold halocline, and the sea ice cover at the surface using a 1D model of the Arctic Ocean water column. Specifically, we focus on the following questions:

1) How do periodic increases in vertical mixing affect the diffusive heat flux through the cold halocline and therefore the sea ice cover at the surface? To what extent can freshwater input at the surface offset the effect of elevated vertical mixing?
2) In what mixing/freshwater regimes does the cold halocline remain stable and how long might it take for the cold halocline to be completely eroded? What effect will this have on the sea ice cover at the surface?

Our approach is similar to that of Killworth and Smith (1984) and Bjork (1989), who use 1D models to investigate the Arctic Ocean halocline and upper-ocean stratification. By using a model that contains only the essential physics needed to represent the competing effects of elevated vertical mixing and freshwater input, we are able to explore a wide parameter space that is applicable to the future Arctic and isolate the role that the changing Arctic Ocean will play in the ongoing melting of Arctic sea ice.

In section 2 of the paper we describe the setup of the 1D model, with the design of our model experiments detailed in section 3. In section 4 we present the results, and we discuss the implications of our findings in section 5. Conclusions are presented in section 6.

2. Model setup

The 1D General Ocean Turbulence Model (Burchard et al. 1999) is used to simulate the upper 500 m of the Arctic Ocean, which is sufficient to cover the region of the water column in which we are interested (i.e., to the core of the Atlantic Water layer). The model is governed by the following temperature and salinity diffusion equations:

$$\frac{\partial \theta}{\partial t} = \frac{\partial}{\partial z}\left(K_z \frac{\partial \theta}{\partial z}\right) - R^{\theta}$$
$$\frac{\partial S}{\partial t} = \frac{\partial}{\partial z}\left(K_z \frac{\partial S}{\partial z}\right) + S_0 - R^{S}, \qquad (1)$$

where θ is potential temperature (henceforth, all temperatures are assumed to be potential temperature), S is salinity, t is time, z is depth, K_z is vertical diffusivity, S_0 is a surface freshwater term equal to the input from rivers and excess precipitation over evaporation, and $R^{\theta}(z)$ and $R^{S}(z)$ represent all other processes not explicitly resolved here that maintain the temperature and salinity stratification. The equations are discretized on a vertical grid with a resolution of 1 m.

The model is initialized with winter (December–February) climatological temperature and salinity profiles from the central Eurasian Basin (Fig. 2a), averaged between 85° and 90°N and 0° and 120°E from the Monthly Isopycnal/Mixed-Layer Ocean Climatology (MIMOC; Schmidtko et al. 2013). The profiles are interpolated from their climatological levels onto a regular 1-m grid and smoothed with a 9-m running mean to minimize sharp gradients. The results of this study are not sensitive to small changes in these initial profiles. Because of the lack of a sea ice model at the surface, the mixed layer temperature can cool below the local freezing point, and we take this cooling to represent sea ice formation.

The model is forced solely by vertical mixing/diffusivity; freshwater input at the surface; and the prescribed, constant-in-time but depth-dependent terms $R^{\theta}(z)$ and $R^{S}(z)$. These represent the net effect of those processes (e.g., lateral advection, surface heat fluxes,

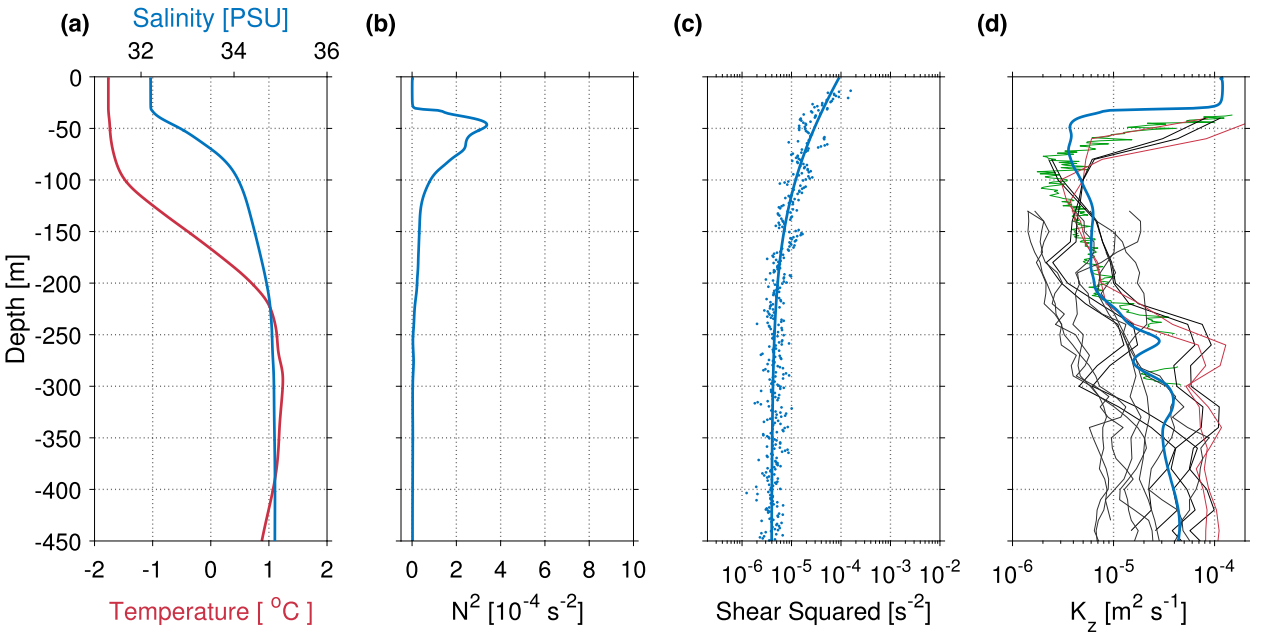

FIG. 2. Initial profiles of (a) temperature and salinity averaged over the central Eurasian Basin region from MIMOC; (b) the corresponding buoyancy frequency; (c) the climatological shear squared, derived from XCP data collected during the North Pole Environmental Observatory surveys between 2008 and 2011 (the blue dots represent the average shear squared values from the 28 individual XCP casts to which the double exponential curve is fitted); and (d) the corresponding vertical diffusivity due to shear instability associated with internal wave breaking (blue line), parameterized through Eq. (2). The thin black lines in (d) show the vertical diffusivity in the Eurasian Basin estimated by Guthrie et al. (2013), and the red and green lines show the vertical diffusivity derived from microstructure observations by Guthrie et al. (2013) and Fer (2009), respectively.

and mean sea ice processes) that balance the vertical diffusivity and freshwater input at the surface in the long-term mean and are determined by restoring θ and S to the mean winter profiles in the control run to ensure a steady state is reached. They are then fixed for the remainder of the study. The details of these terms are described in more detail below.

We assume that the vertical diffusivity in Eq. (1) is a function of only the shear instability associated with internal wave breaking and is parameterized in terms of the Richardson number (Ri; Pacanowski and Philander 1981):

$$K_z = \frac{K_z^{\max} + \nu_b(1+\alpha \mathrm{Ri})^n}{(1+\alpha \mathrm{Ri})^{n+1}} + K_z^b, \qquad (2)$$

where $\mathrm{Ri} = N^2/S^2$ is a function of the buoyancy frequency (N^2; Fig. 2b) and the shear squared [$S^2 = (\partial u/\partial z)^2 + (\partial v/\partial z)^2$; Fig. 2c], $K_z^{\max}$ is the maximum diffusivity, K_z^b is the background diffusivity, ν_b is the background viscosity, and α and n are tuning parameters. This parameterization was specifically chosen as it allows the diffusivity to be sensitive to both changes in the freshwater input and the periodic increases in vertical mixing. Physically, if the stratification is strong (significant freshwater input, large N^2) and the shear is weak (small S^2), the Richardson number is large and the diffusivity is small, with K_z tending toward K_z^b. Conversely, if the stratification is weak and the shear is strong, the Richardson number is small and the diffusivity tends toward $K_z^{\max}$.

Observations in the Arctic (e.g., Halle and Pinkel 2003; Pinkel 2005; Dosser et al. 2014) have shown that the internal wave field is highly episodic in nature, and the shear instability associated with internal wave breaking exhibits high-frequency variability both in time and space. However, it is challenging to incorporate this variability directly into models because of the limitations associated with their much coarser space and time resolutions. As Lique et al. (2014) have shown that these episodic mixing events act to increase the magnitude of the average background mixing, and as we would expect the Arctic internal wave field to move closer to a more typical midlatitude Garrett–Munk (Garrett and Munk 1975) internal wave field during longer ice-free periods (i.e., with stronger mean background shear and diffusivity), we follow the classical approach used by models that do not resolve the relevant time and space scales by defining the initial shear squared profile (Fig. 2c) to be the average of 28 individual u and v velocity shear profiles collected during the North Pole Environmental Observatory airborne hydrographic surveys between

2008 and 2011 (Guthrie et al. 2013). The u and v velocity data from each of the XCP casts are interpolated onto a regular 1-m grid, and the corresponding u and v velocity shear profiles are calculated from overlapping 8-m bins, with a resolution of 1 m. The absolute values from each of the 28 u and v velocity shear profiles are then averaged to produce a single u and v velocity shear profile, to which curves of the form

$$\frac{\partial u}{\partial z} \text{ or } \frac{\partial v}{\partial z} = ae^{bz} + ce^{dz}, \tag{3}$$

where z is depth and a, b, c, and d are constants fitted in order to smooth sharp gradients. These fitted velocity shear profiles are then integrated from the bottom boundary at 500 m (where the velocity is set to zero) to the surface, to produce the corresponding idealized u and v velocity profiles with which the model is forced. It is important to note that although the magnitude and the shape of the shear profile should also scale with the changing stratification throughout each model run, we do not incorporate this effect into our model on the assumption that any change in shear due to the evolving stratification will likely be significantly smaller than the change in shear that we implement manually to enhance the vertical mixing (discussed in section 3). This assumption allows us to keep the problem tractable and eliminates the effect of complex feedbacks between shear and stratification that are still poorly pinned down.

To match the initial profile of K_z (Fig. 2d) to observations of diffusivity from the Eurasian Basin (Fer 2009; Guthrie et al. 2013), K_z^b was set to the observed value of $2.0 \times 10^{-6}\,\mathrm{m^2\,s^{-1}}$ (Rainville and Winsor 2008); ν_b was set to $2.0 \times 10^{-5}\,\mathrm{m^2\,s^{-1}}$ (Large et al. 1994); α was set to 1; n was set to 2; and $K_z^{\max}$ was set to $10^{-4}\,\mathrm{m^2\,s^{-1}}$, the maximum plausible value in the ocean interior (Munk 1966; Munk and Wunsch 1998). Figure 2d shows the good agreement between the initial K_z profile and the observations. In the mixed layer, K_z is large (approximately $10^{-4}\,\mathrm{m^2\,s^{-1}}$) because of the weak stratification and strong shear (Figs. 2b,c). Below the mixed layer and into the cold halocline, the stratification increases and the shear decreases, reducing K_z to a minimum of $2.0 \times 10^{-6}\,\mathrm{m^2\,s^{-1}}$. Beneath the cold halocline, the weakening stratification drives a general trend toward higher K_z, despite the lower shear.

At present, freshwater input to the Arctic from rivers and excess precipitation over evaporation equals $6400\,\mathrm{km^3\,yr^{-1}}$ (Haine et al. 2015). When divided by the area of the Arctic ($9.7 \times 10^6\,\mathrm{km^2}$), this corresponds to an average input of $2.12 \times 10^{-8}\,\mathrm{m\,s^{-1}}$ (based on a 360-day model year), which is applied at the surface of our model. Throughout this study we assume that the freshwater input from rivers is distributed evenly throughout the Arctic Ocean. To rapidly distribute this freshwater over the mixed layer, an ocean stress of $0.044\,\mathrm{N\,m^{-2}}$ is applied at the surface, which agrees well with the average winter ocean stress over the Eurasian Basin from the Nucleus for European Modelling of the Ocean–Louvain-la-Neuve (NEMO-LIM) coupled ice–ocean model (Lique and Steele 2012). In all model runs, the effect of the wind stress on the vertical diffusivity is restricted to the upper 31 m, which is the depth of the mixed layer in the climatological profiles (the depth of the mixed layer throughout this study is defined as the depth at which the density has increased by $0.01\,\mathrm{kg\,m^{-3}}$ from the surface value). This choice has been made to ensure that changes to the diffusivity and thus the vertical heat flux below this depth reflect only the interplay between the elevated diffusivity and the enhanced freshwater input. In all model experiments the mixed layer depth is free to evolve in response to the changing heat flux/fresh water input.

The lateral advection of ''new'' water masses into the 1D domain, as well as all other processes such as surface heat fluxes and the salt fluxes from sea ice formation and melt, that balance the vertical diffusivity and freshwater input at the surface in the long-term mean are taken into account through the depth-dependent terms $R^\theta(z)$ and $R^S(z)$. We have chosen to exclude the effect of seasonality and future changes in the strength of these processes (which likely depend on poorly understood processes such as the effect of sea ice retreat on shelf and shelf edge processes, changes in the absorption of solar radiation into the upper ocean, variability and change in advective pathways, and shifts in the annual cycle of sea ice cover/thickness) by fixing the magnitude of the terms in each model run to be equal to the relaxation required to reach a steady state in the control run:

$$\begin{aligned} R^\theta(z) &= \frac{1}{\tau}\overline{[\theta(t,z) - \theta(0,z)]} \\ R^S(z) &= \frac{1}{\tau}\overline{[S(t,z) - S(0,z)]}, \end{aligned} \tag{4}$$

where the overbar represents a time average over the control run, τ is the relaxation time scale (12 days), and $[\theta(t, z) - \theta(0, z)]$ and $[S(t, z) - S(0, z)]$ are the differences between the temperature and salinity profiles at time t and the initial temperature and salinity profiles ($t = 0$). This choice allows us to isolate and understand the effect that only elevated vertical mixing and enhanced freshwater input will have on the Arctic stratification and thus the sea ice cover at the surface. The exact shape of the R terms (solid lines in Fig. 3) is set by the vertical variation in convergence/divergence of the vertical heat and salt fluxes. Small vertical variations in

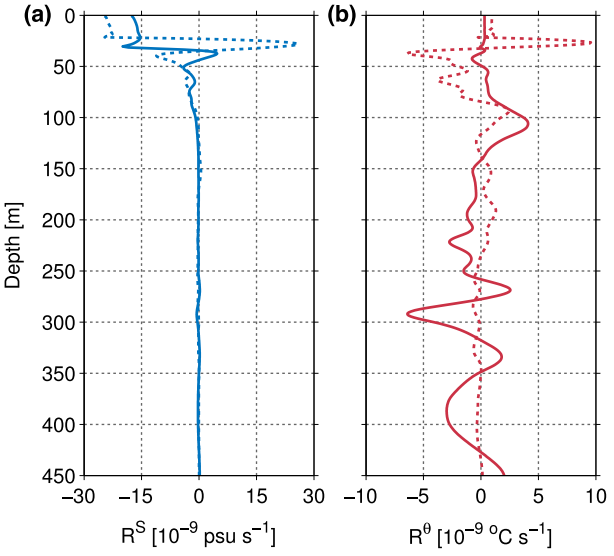

FIG. 3. Magnitude of (a) $R^S(z)$ and (b) $R^\theta(z)$ in the Eurasian Basin (solid lines) and the Canadian Basin (dotted lines). The strength of these terms is determined by relaxing θ and S in the control run to the initial winter profiles to ensure a steady state is reached. They are prescribed in all subsequent perturbation runs. Note that negative values of $R^S(z)$ and $R^\theta(z)$ indicate salinification and warming, respectively.

temperature found near the Atlantic Water temperature maximum introduce vertical structure into the initial K_z profile and hence into these terms. However, when integrated over the full depth ranges of the different water masses, their net effect is to cool and remove freshwater from the mixed layer, while warming and increasing the salinity of the Atlantic Water layer. Indeed, by defining the boundary between the Atlantic Water layer and the upper cold halocline at 90 m and calculating the integrated heating over these two layers as

$$Q = -\int R^\theta(z)\rho_0 C_p \, dz, \tag{5}$$

where ρ_0 is the density (1027 kg m^{-3}) and C_p is the ocean specific heat capacity (3985 J kg^{-1} K^{-1}), the net effect of the temperature term $R^\theta(z)$ results in a warming over the Atlantic Water layer of 0.15 W m^{-2} and a fully compensating cooling over the cold halocline [i.e., $R^\theta(z)$ integrates to zero]. This compares well to the observational estimates of the vertical heat flux from the Atlantic Water layer of Timmermans et al. (2008), Sirevaag and Fer (2012), and Shaw and Stanton (2014). It should be noted that there is no flux of salt or heat through the bottom boundary at 500 m.

Because we adopt a simple 1D representation of the Arctic Ocean, there are a number of important processes that cannot be directly resolved in our model. As $R^\theta(z)$ and $R^S(z)$ are fixed in time, we cannot consider the effect that any interplay between enhanced vertical mixing and seasonality in the Arctic mixed layer depth (which is poorly constrained; Peralta-Ferriz and Woodgate 2015), winter convection (due to surface heat fluxes and sea ice formation), and the processes that form the cold halocline may have on the sea ice cover at the surface, while the effects of long-term changes in the advection of water masses around the Arctic are also ignored. In addition, despite the net effect of the surface heat flux being included within the $R^\theta(z)$ and $R^S(z)$ terms, we do not consider the effect of changes in surface heating. Although the surface heat flux is likely to play a major role in the future sea ice budget of the Arctic by heating the upper ocean during ice-free periods (e.g., Timmermans 2015), we are primarily interested in isolating the role that elevated vertical mixing and deeper changes to the Arctic Ocean water column will play in the ongoing melting of Arctic sea ice. Finally, the effects of ice–ocean interactions at the surface are not included, as Barthélemy et al. (2015) show that the parameters required for brine rejection parameterizations are poorly observed and constrained. Possible implications of these missing processes for our results will be discussed in section 5.

3. Experimental design

To explore how the competition between periodic increases in vertical mixing during ice-free periods and elevated freshwater input to the Arctic Ocean will affect the stratification and sea ice cover over the coming decades, we perturb four parameters in our model. These are 1) the magnitude of the velocity shear during ice-free periods, 2) the depth to which this elevated velocity shear penetrates, 3) the length of the ice-free period, and 4) the magnitude of the freshwater input. Since the future trends in the magnitude of these parameters are unknown, we perturb them idealistically through a wide parameter space that is broadly applicable to the future Arctic. For each unique set of parameters, the model is initialized from the profiles in Fig. 2 and run for 50 years, which represents the period of time over which the Arctic is expected to have become predominantly ice-free in summer (Wang and Overland 2009).

The magnitude of velocity shear during ice-free periods is perturbed by multiplying the initial velocity shear profiles by a factor of 1–6 (referred to as the shear factor or SFac), matching the change in the velocity shear observed by Rainville and Woodgate (2009) during ice-free periods in the Chukchi Sea. The shear factor is not constant throughout the water column, but is at its maximum at the surface and decreases smoothly to 1 at the depth to which the elevated velocity shear penetrates (referred to as ZMax). Based on the initial

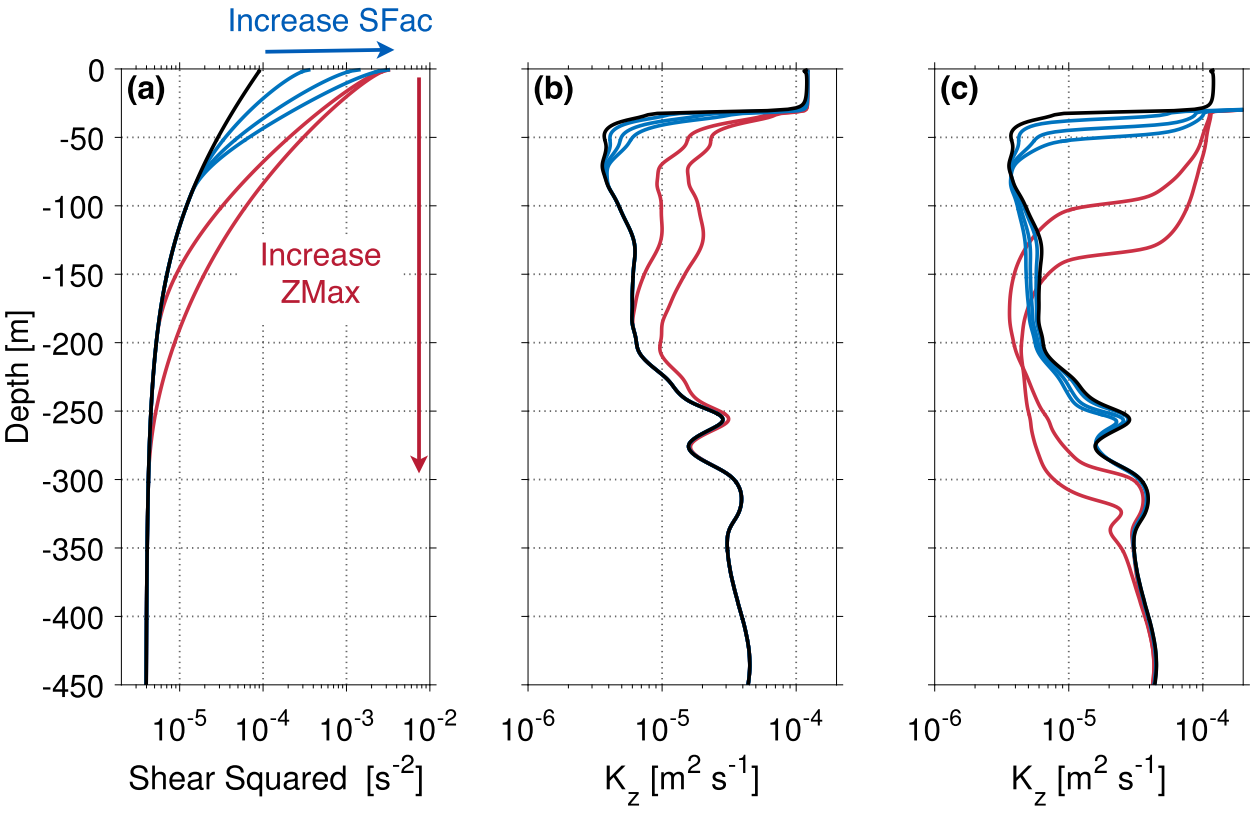

FIG. 4. The effect on (a) the shear squared profile and (b) the vertical diffusivity profile when the velocity shear profiles from the control run (black profiles in each panel) are multiplied by an SFac of 2, 4, or 6 down to a ZMax of 90 m (blue lines), and by an SFac of 6 down to a ZMax of 195 or 300 m (red lines). (c) The effect that the same perturbations made in (a) have on the vertical diffusivity after 50 years of a model run in which they have been applied for 6 months of each year with no change in the freshwater input. Note that the very high diffusivities seen in the mixed layer in (c) are due to the ocean stress applied at the surface.

profiles, ZMax is defined as either 90 m (the base of the cold halocline), 300 m (the core of the Atlantic Water layer), or 195 m (midway between the base of the cold halocline and the core of the Atlantic Water layer). An example of the effect that these perturbations have on the shear squared and diffusivity profiles can be seen in Fig. 4. Although the perturbations to K_z can initially be quite small (Fig. 4b), the cumulative effect over a model run is much more significant as the stratification changes throughout the water column (Fig. 4c).

The length of the ice-free period is either 2, 4, or 6 months, reflecting the general trend toward a thinner and less extensive sea ice cover, with the earlier occurrence of melt onset and later freeze-up (Markus et al. 2009; Overland and Wang 2013; Pinker et al. 2014; Wang and Overland 2015). During these ice-free periods the model is forced with the perturbed velocity shear profiles (i.e., Fig. 4a), and over the remainder of the year the model is forced with the control velocity shear profiles (i.e., Fig. 2c). It should be noted that these "ice-free periods" can also be interpreted as periods during which a less extensive but still present sea ice cover is acting to enhance the transfer of wind momentum into the upper ocean [as discussed by Tsamados et al. (2014), Martin et al. (2014), and Davis et al. (2014)].

The freshwater input from river runoff and positive $P - E$ is perturbed by applying annual anomalies at the surface that represent a 0%–30% increase from present-day values, spanning the change projected by state-of-the-art climate models in the Arctic freshwater input over the next 50 years (Vavrus et al. 2012; Bintanja and Selten 2014; Haine et al. 2015). The annual anomaly is distributed equally throughout the year and is applied at the surface grid cell.

By varying these four parameters through a wide parameter space, we have run a total of 378 simulations. In the following, we present the most important results, showing relevant examples rather than focusing on the whole set of simulations.

4. Results

Arctic sea ice is sensitive to changes in the diffusive heat flux and the extent to which the mixed layer is isolated from the heat contained within the Atlantic Water layer.

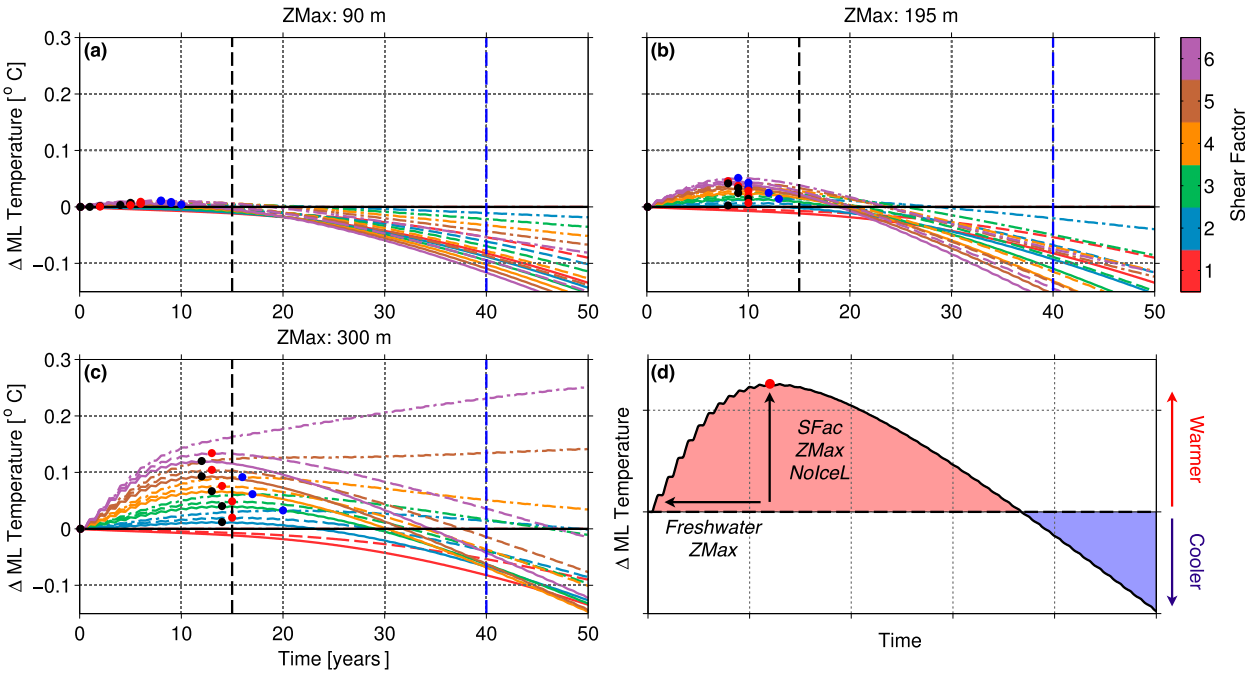

FIG. 5. Time series of the deviation in mixed layer temperature from the constant control value for model runs in which the velocity shear profiles have been perturbed for 6 months of each year down to a ZMax of (a) 90 m, (b) 195 m, and (c) 300 m. The color of each line in (a)–(c) represents the shear factor, and the solid, dashed, and dot–dashed lines represent a 30%, 15%, and 0% increase in the freshwater input, respectively. The colored dots mark the maximum deviation in the mixed layer temperature, with the black, red, and blue dots corresponding to a 30%, 15%, and 0% increase in the freshwater input, respectively. If a symbol is not present for a specific model run, it indicates that the mixed layer temperature has not reached a maximum within 50 years. The black and blue dashed vertical lines mark 15 and 40 years of each model simulation, respectively. (d) Schematic showing the mechanisms that control the timing and magnitude of the maximum deviation in the mixed layer temperature (red dot). SFac refers to the shear factor, ZMax refers to the depth to which the elevated shear penetrates, NoIceL refers to the length of the ice-free season, and Freshwater refers to the magnitude of the freshwater input anomaly.

In this section we explore how and why these parameters will likely evolve over the coming decades.

a. Mixed layer temperature and the diffusive heat flux

For all model runs in which the velocity shear is elevated (i.e., excluding a shear factor of one), there is an initial increase in mixed layer temperature (Fig. 5). We have chosen to show the results from only the longest ice-free period, as the mechanisms that control mixed layer temperatures are independent of the length of the ice-free period and are equally applicable to the remainder of the parameter space. The magnitude of the change in mixed layer temperature depends predominantly on the shear factor and the depth of ZMax. For example, when ZMax is 300 m (Fig. 5c), the maximum deviation in mixed layer temperature for model runs with a shear factor of 6 is 0.25°C (purple dot–dashed line), compared to a maximum of only 0.03°C for model runs with a shear factor of 2 (light blue dot–dashed line). In contrast, when ZMax is 90 m (Fig. 5a), the maximum deviation in mixed layer temperature does not exceed 0.01°C.

In our model, where the mean effect of surface heat fluxes and sea ice processes are combined with lateral advection in the $R^{\theta}(z)$ and $R^{S}(z)$ terms, the mixed layer heat budget can be written as

$$h\left\langle \frac{\partial \theta}{\partial t} \right\rangle = -h\langle R^{\theta}(z)\rangle + K_z \frac{\partial \theta}{\partial z_{(z=-h)}}, \tag{6}$$

where h is the depth of the mixed layer, $\langle\ \rangle$ indicates a depth average over the mixed layer, the first term on the right-hand side represents the change in mixed layer temperature due to $R^{\theta}(z)$, and the second term represents the change in mixed layer temperature due to the diffusive heat flux at the base of the mixed layer. As $R^{\theta}(z)$ is constant in our model, variability in mixed layer temperature depends solely on changes in the diffusive heat flux at the base of the mixed layer. We therefore deduce from Fig. 5 that during the initial phase of each model run, the diffusive heat flux is enhanced compared to the control run, and excess heat is accumulating in the mixed layer.

After a number of years, however, Fig. 5 shows that the mixed layer begins to cool in many model runs, and thus the magnitude of the diffusive heat flux in these simulations must have decreased with respect to the control run. The point in time at which this occurs in each model run is marked with a colored dot and is determined primarily by the magnitude of the freshwater input and the depth of ZMax. For example, for model runs with a ZMax of 300 m (Fig. 5c) and no change in the freshwater input (blue dots), the maximum mixed layer temperature occurs after 15–20 years. In comparison, with a freshwater input anomaly of 30% (black dots), the maximum mixed layer temperature is reached between 11 and 14 years. When ZMax is only 90 m (Fig. 5a), the maximum mixed layer temperature occurs within the first 10 years, irrespective of the freshwater input. For the two model runs in Fig. 5c with an SFac of 5 and 6 and a 0% increase in the freshwater input (i.e., the brown and purple dot–dashed lines, respectively), the positive trend in mixed layer temperature does not reverse for at least another 50 years.

To understand the changes in the diffusive heat flux across parameter space, we examine a number of individual model runs after 15 and 40 years (black and blue dashed lines in Fig. 5, respectively) that span the full range of trajectories in mixed layer temperature. The initial increase in mixed layer temperature (top inset in Fig. 6a) in all model runs in which the velocity shear is perturbed (orange, purple, and green profiles) is due to larger diffusivities in the upper 100 m (Fig. 6d) driving an enhanced diffusive heat flux. In contrast, when only the freshwater input is increased (blue profile), the mixed layer cools as the stronger stratification decreases the diffusivity and reduces the magnitude of the diffusive heat flux. The initial increase in mixed layer temperature depends strongly on the depth to which the elevated shear penetrates, as the diffusive heat flux depends on both the diffusivity and the strength of the temperature gradient. Deeper mixing can interact with the much stronger Atlantic Water layer temperature gradient (below ≈100 m) and can thus drive significantly more heat into the mixed layer. For example, for two model runs with the same shear factor and freshwater input, the change in mixed layer temperature after 15 years is 0.16°C when ZMax is 300 m (orange profile), compared to only 6×10^{-3}°C when ZMax is 90 m (purple profile). In contrast, the elevated freshwater input has little effect, with a 30% increase reducing the maximum change in mixed layer temperature by only 0.04°C (cf. the orange and green profiles). Overall, in comparison to the annual change in mixed layer temperature driven by the absorption of solar radiation (>1°C; Perovich et al. 2008; Steele et al. 2011), the change in mixed layer temperature after 15 years is insignificant.

The elevated diffusivity also affects the stratification throughout the water column. As evident in Fig. 6c, a deepening of the halocline has reduced the strength of the stratification over the upper water column to zero (associated with a weakening of the salinity gradient), while deeper in the water column the stratification has increased because of the strengthening of the salinity gradient. Consequently, the depth of maximum stratification has increased from 44 m in the control run to a maximum of 118 m, and the diffusivity has decreased between 200 and 300 m.

After 40 years, Fig. 6e shows that the mixed layer has cooled in all model runs with respect to the control run, except when ZMax is 300 m and there is no increase in the freshwater input (orange profile; in this case the diffusivity has continued to increase in the upper water column, maintaining the vertical heat flux, and deepening the mixed layer, which has entrained warm water from the Atlantic Water layer). Over the remaining model runs, the mixed layer has cooled because of the continued strengthening of the stratification over the Atlantic Water layer (i.e., between ≈100 and 300 m), decreasing the magnitude of the diffusivity (Figs. 6d,h) and thus the diffusive heat flux to the base of the mixed layer. The stratification has strengthened because of both the ongoing freshwater input at the surface and the deepening of the halocline. In addition to cooling the mixed layer, the reduced diffusive heat flux also causes the Atlantic Water layer to warm (bottom inset in Fig. 6e; Nummelin et al. 2015). It must be remembered that, because of the lack of a sea ice model at the surface, the mixed layer can cool below the local freezing point, and this cooling is taken to represent sea ice formation. The magnitude of this sea ice formation is discussed in more detail later in this section.

To summarize the results thus far, the schematic presented in Fig. 5d highlights the dominant processes responsible for determining the evolution of the diffusive heat flux and mixed layer temperature. Elevated shear drives an initial increase in mixed layer temperature because of larger diffusivities enhancing the diffusive heat flux across the base of the mixed layer. As the diffusive heat flux depends on both the diffusivity and the strength of the temperature gradient, the change in mixed layer temperature is greater for higher shear factors and when the elevated shear penetrates deep into the Atlantic Water layer. Furthermore, the increase in mixed layer temperature is greater for longer ice-free seasons, as the integrated heat flux over the year is larger. The most important result, however, is that after a period of time, strengthening of the stratification over the Atlantic Water layer (due to the

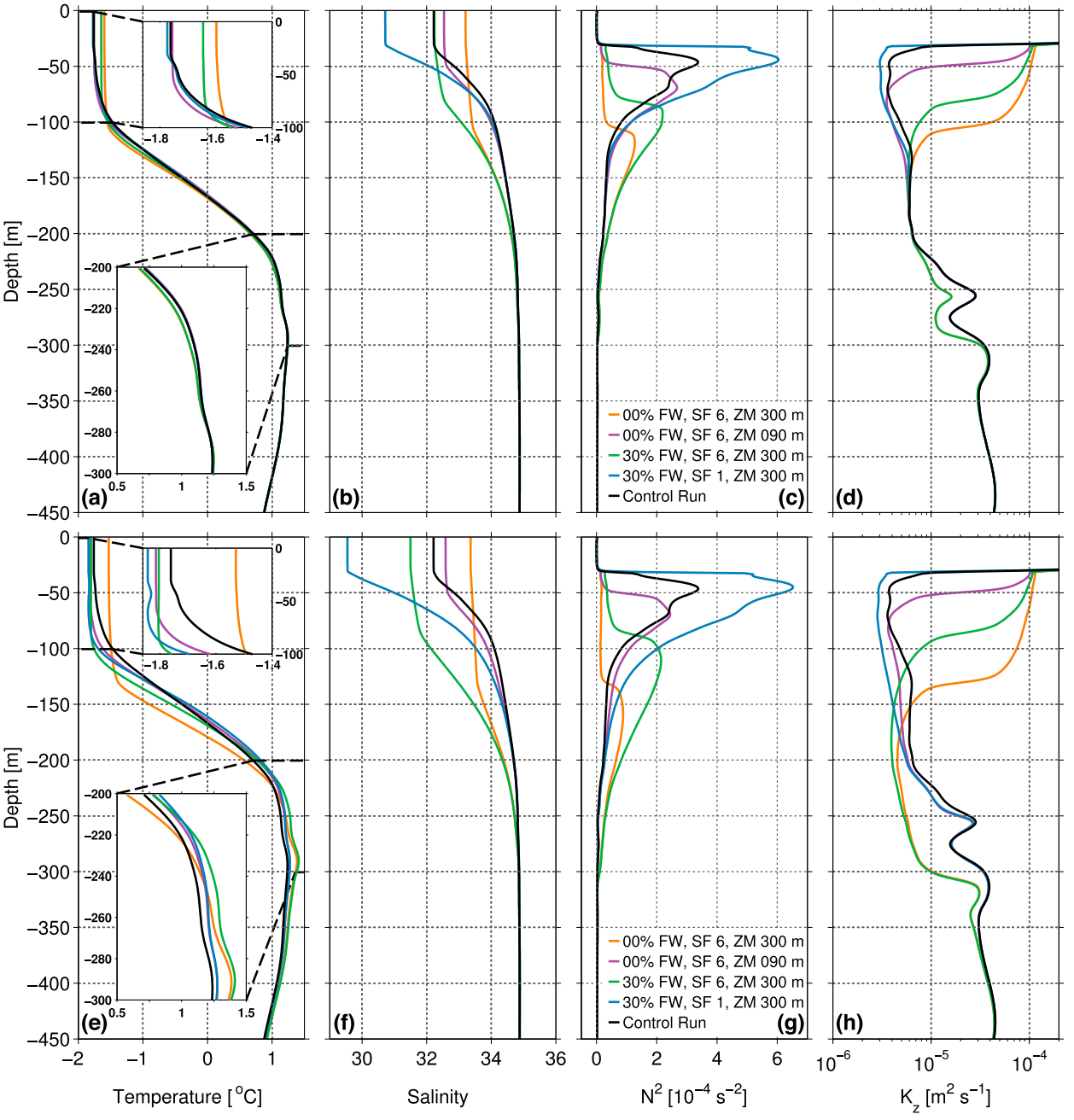

FIG. 6. Profiles of (a),(e) temperature; (b),(f) salinity; (c),(g) buoyancy frequency; and (d),(h) diffusivity for a number of individual model runs. Profiles (a)–(d) show the water column structure after 15 years of each model run (black dashed line in Fig. 5), and profiles (e)–(h) show the water column structure after 40 years (blue dashed line in Fig. 5). In the legend, FW refers to the magnitude of the freshwater input anomaly, SF refers to the magnitude of the shear factor, and ZM refers to the depth of ZMax.

elevated freshwater input and the deepening of the halocline) weakens the diffusivity, and thus the decrease in the upward diffusive heat flux causes the mixed layer to cool. The time required for this to occur is determined by the extent to which the stratification over the Atlantic Water layer must strengthen before it balances the increased diffusivity and elevated diffusive heat flux higher in the water column. To characterize the details of this relationship, the change from the control run in the magnitude of the potential energy anomaly over the Atlantic Water layer (i.e., between 100 and 300 m) at the time of the maximum mixed layer

temperature is calculated from (Simpson and Bowers 1981):

$$\Delta\Phi = \frac{g}{h_{\mathrm{AW}}}\left[\int [\overline{\rho}_{\mathrm{AW}}(t) - \rho(t,z)](D-z)\,dz - \int [\overline{\rho}_{\mathrm{AW}}(0) - \rho(0,z)](D-z)\,dz\right], \quad (7)$$

where g is the acceleration due to gravity; h_{AW} is the thickness of the Atlantic Water layer; $\overline{\rho}_{\mathrm{AW}}$ is the mean density over the Atlantic Water layer; $\rho(z)$ is the in situ density; t is the time of maximum mixed layer temperature; and $(D - z)$ is height above the reference level D, which in this case is 500 m. For model runs in which the velocity shear is elevated for 6 months of each year, a near-linear relationship exists between the maximum deviation in the mixed layer temperature and the change in the strength of the stratification over the Atlantic Water layer at the time of the maximum mixed layer temperature (Fig. 7; note that the same relationship also holds when the length of the ice-free season is shorter). As would be expected, when SFac is small, ZMax is shallow and the change in the freshwater input is large, the extent to which the stratification over the Atlantic Water layer must strengthen before it can balance any increase in the diffusive heat flux higher in the water column is generally small, and thus both the maximum change in the mixed layer temperature (Fig. 7) and the period of time before the mixed layer begins to cool are small (Fig. 5). On the other hand, while a greater increase in the stratification over the Atlantic Water layer is required to balance larger values of SFac or ZMax, Fig. 5 shows that the timing of the maximum mixed layer temperature for a given ZMax is generally earlier when SFac is larger, suggesting that strongly elevated diffusivities can deepen the halocline and strengthen the stratification over the Atlantic Water layer faster.

Following Steele et al. (2008, 2011), the effect of the elevated diffusive heat flux on the sea ice cover is quantified by calculating the change in the mixed layer heat content (ΔH_c) from the initial profile ($t = 0$) after $t = 15$ and $t = 40$ years of each model run:

$$\Delta H_c = \rho_0 C_p \left\{\int_{z=-h}^{z=0} [\theta(t) - \theta_f(t)]\,dz - \int_{z=-h}^{z=0} [\theta(0) - \theta_f(0)]\,dz\right\}, \quad (8)$$

where θ_f is the in situ freezing point based on the average mixed layer salinity at time t. The equivalent net quantity of sea ice that can be melted/formed because of this change in heat content is

$$\Delta h_I = \frac{\Delta H_c}{\rho_I L_I}, \quad (9)$$

where ρ_I is the density of sea ice (900 kg m^{-3}) and L_I is the latent heat of fusion of sea ice (3×10^5 J kg^{-1}).

Figure 8 shows that after 15 years, the effect of the elevated diffusive heat flux is limited, with a maximum equivalent net sea ice loss of only 12 cm (bottom right in Fig. 8c). When the elevated shear extends to a depth of either 195 or 300 m, the contour lines showing the change in mixed layer temperature are aligned parallel to the freshwater axes, highlighting the limited role played by freshwater input in determining the initial increase in mixed layer temperature. In contrast, when ZMax is 90 m, or the freshwater input is significant, the decrease in mixed layer heat content is equivalent to the net formation of 4 cm of sea ice. This formation is driven by the combination of cooler mixed layer temperatures compared to the control run and an increase in the local freezing point due to the input of freshwater. This second process is particularly important for the equivalent net sea ice formation seen to the right of the magenta line in Figs. 8a–c, where the input of freshwater has raised the local freezing point faster than the rate at which the mixed layer temperature has increased. It must be noted that a snapshot at 15 years is after the maximum mixed layer temperature has been reached for model runs with a ZMax of either 90 or 195 m (Fig. 5). However, at the point of maximum mixed layer temperature for each ZMax (8 and 9 years for 90 and 195 m, respectively), the equivalent net loss of ice is only 2 and 5 cm, respectively.

After 40 years, Fig. 8 shows that the parameter space is dominated by net sea ice formation, with ongoing sea ice melt limited to model runs in which strongly elevated shear extends to the Atlantic Water layer and there is little change in the freshwater input. In this case, the maximum equivalent net sea ice loss is ≈16 cm (bottom right of Fig. 8f). The magnitude of the equivalent net sea ice formation seen throughout the remainder of the parameter space is determined by the magnitude of the freshwater input (the colored contours lie parallel to the SFac axes) and reaches a maximum of 11 cm. It is interesting to note that when ZMax is either 90 or 195 m, runs with higher shear factors tend to exhibit a greater decrease in mixed layer temperature from the control run for a given freshwater input, but this is not reflected in the sea ice formation. In these cases, the decrease in the mixed layer salinity is smaller compared to runs with a lower shear factor, and thus the ability to form more sea ice from the cooler mixed layer temperature is offset by the lower freezing point.

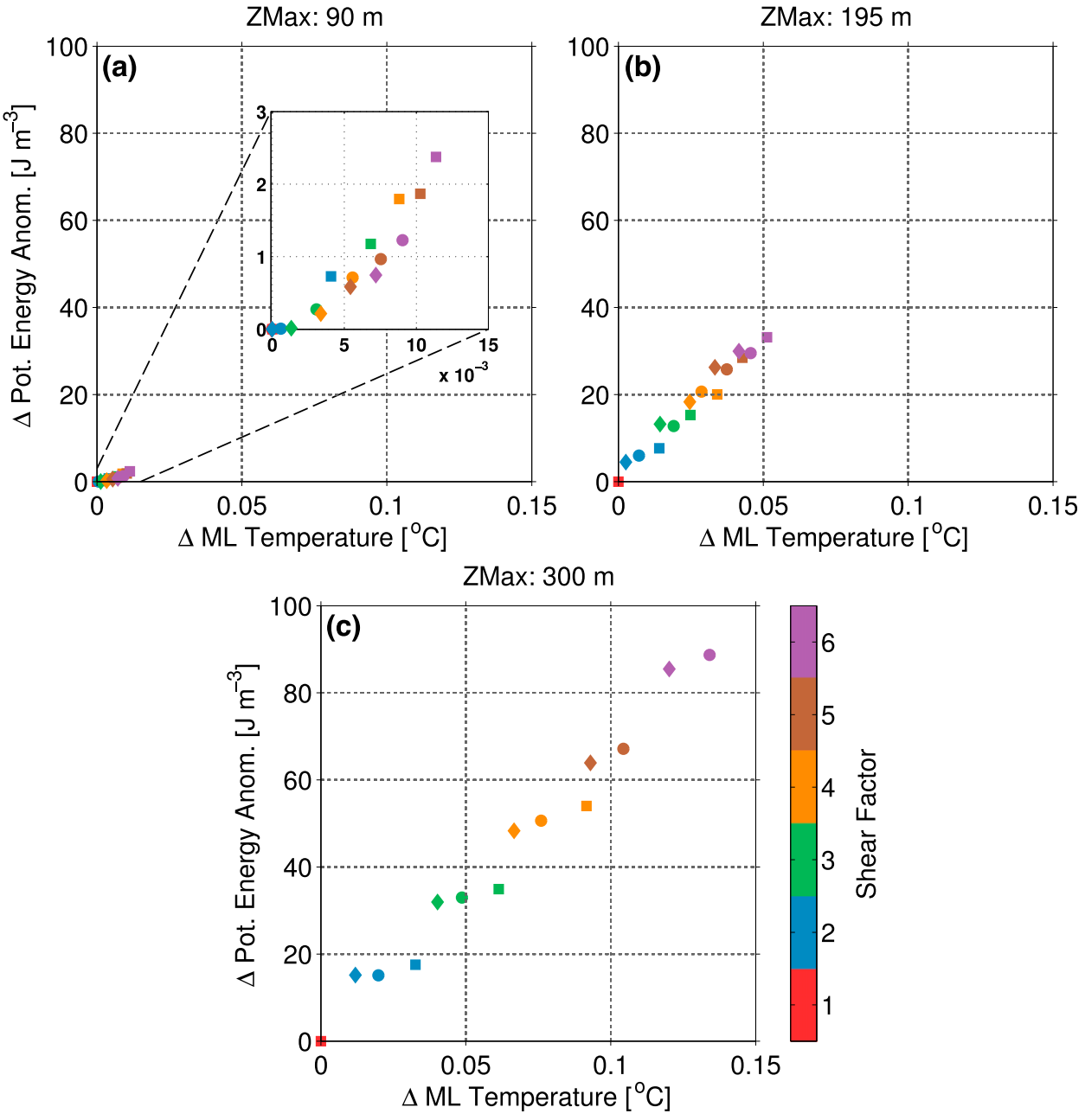

FIG. 7. Relationship between the maximum deviation in the mixed layer temperature and the change in the magnitude of the potential energy anomaly over the Atlantic Water layer at the time of maximum mixed layer temperature, for model runs in which the velocity shear has been elevated for 6 months of each year down to a ZMax of (a) 90, (b) 195, and (c) 300 m (the same relationship also holds when the length of the ice-free season is shorter). The color of each symbol represents the shear factor, while the diamonds, circles, and squares represent a 30%, 15%, and 0% increase in the freshwater input, respectively.

Overall, it is important to note that the elevated diffusive heat flux in our model melts significantly less sea ice than the other major processes responsible for sea ice melt in the Arctic, and because of the isolating effect of the sea ice cover that is not simulated directly in our model [i.e., as the mixed layer warms (cools) and sea ice is melted (formed), the extent to which the ocean is isolated from the atmosphere will decrease (increase), enhancing (reducing) the surface heat flux and acting as a negative feedback], the estimates of ice formation and melt presented here must be considered as upper-bound estimates.

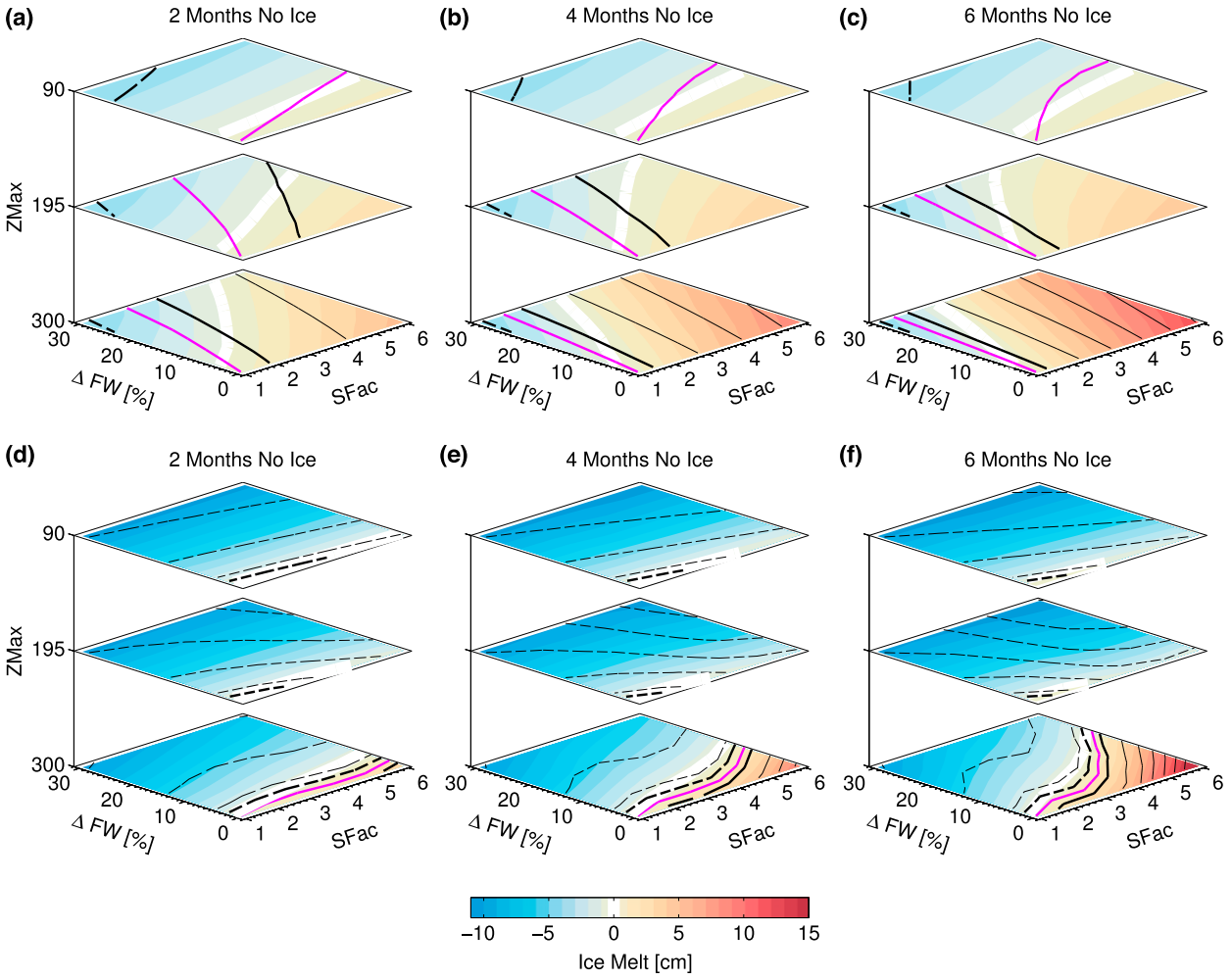

FIG. 8. Thickness of ice (color contours) that could be melted/formed because of the change in the mixed layer heat content after (a)–(c) 15 years and (d)–(f) 40 years of each model run, plotted as a function of the shear factor (SFac) and the freshwater anomaly at the surface (ΔFW). The individual columns represent the different lengths of the ice-free season, and the individual layers in each column represent the three different depths to which the elevated shear penetrates (i.e., ZMax). Negative ice melt indicates ice formation. Overlain are contours showing the deviation in the mixed layer temperature from the control run. Solid contours indicate an increase in the mixed layer temperature, and dashed contours indicate a decrease in the mixed layer temperature. The contour interval is 0.03°C, with the zero contour marked in magenta and the first contour (i.e., ±0.03°C) marked in bold.

b. Cold halocline strength and heat entrainment

In the presence of a cold halocline, heat from the top of the Atlantic Water layer cannot be directly entrained into the mixed layer because of the strong stratification barrier, and the vertical heat flux is dominated by diffusive fluxes. In this section we explore how the competing effects of elevated vertical mixing and enhanced freshwater input may affect the stability of the cold halocline, and whether it weakens sufficiently to allow warm Atlantic Water to be directly entrained into the mixed layer.

Similar to the approach of Bourgain and Gascard (2011), the strength of the cold halocline is represented by the magnitude of the density gradient [N^2 (s^{-2})] found between the base of the mixed layer and the top of the Atlantic Water layer thermocline (i.e., the bottom of the cold halocline), calculated as

$$N^2 = \frac{g}{\rho_0}\frac{\rho_2 - \rho_1}{z_2 - z_1}, \tag{10}$$

where g is the acceleration due to gravity (9.81 $m\,s^{-2}$) and ρ_2 and ρ_1 are the densities at the top of the Atlantic Water layer thermocline (z_2) and the base of the mixed layer (z_1), respectively. The top of the Atlantic Water layer thermocline is defined as the depth at which the large-scale temperature gradient first exceeds 8.5×10^{-3} °C m^{-1}. After 40 years, Fig. 9 shows that for large

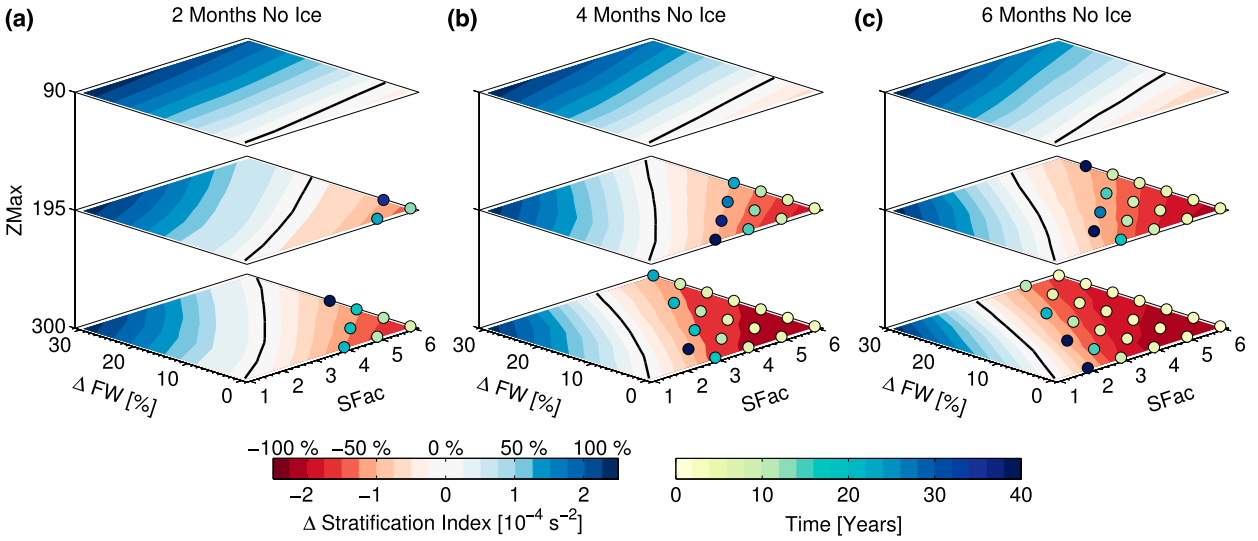

FIG. 9. Deviation from the control run in the strength of the stratification associated with the cold halocline after 40 years of each model run, plotted in the same format as Fig. 8. The solid black line indicates the zero contour for the deviation in the stratification index. Each model run in which the cold halocline is no longer present after 40 years is indicated with a dot. The color of the dot indicates how long it takes for the cold halocline to be fully eroded.

increases in the shear that extend deep into the water column, the strength of the cold halocline decreases, with the density gradient weakening by up to 94% from the control run (i.e., the elevated diffusivity has deepened the halocline, removing the stratification barrier between the mixed layer and the Atlantic Water layer; orange profile in Fig. 6). In contrast, when the freshwater input is large (e.g., the blue profile in Fig. 6) or the elevated shear does not penetrate below 90 m, the strength of the cold halocline increases. Although it is challenging to define a theoretical cutoff in θ–S space below which the stratification barrier associated with the cold halocline is no longer present, a visual examination of individual θ and S profiles suggests that the cold halocline has been fully eroded once the stratification index has decreased by ≈40%. Figure 9 shows that when ZMax is only 90 m, the cold halocline remains present, irrespective of the shear factor. In contrast, when the shear is strongly elevated and extends to a depth of 300 m for up to 6 months of each year, the cold halocline can be fully eroded within 5–10 years (e.g., see the orange profile in Fig. 6b).

Once the cold halocline has been fully eroded, the stratification barrier that isolates the mixed layer from the Atlantic Water layer is no longer present, and the sea ice cover at the surface is sensitive to the episodic effects of wind and storm-generated overturning and convective instability. For example, sea ice formation in the Arctic releases salt into the mixed layer, increasing the density and triggering haline convection (Martinson and Steele 2001). In the absence of a cold halocline this convection can penetrate all the way to the top of the Atlantic Water layer, entraining water that is above the freezing point and thus preventing the continued formation of sea ice at the surface. To quantify the impact of this entrainment heat flux, we employ the parameterization developed by Martinson (1990) and Martinson and Iannuzzi (1998). The parameterization assumes that the thermal forcing for ice growth (F_L) is given by the difference between the ice to atmosphere heat flux (F_A, taken as 25 W m^{-2}; Overland et al. 1997), and the ocean to ice heat flux (F_H), which is parameterized as the average diffusive heat flux over the halocline (Fig. 10):

$$F_L = F_A - F_H,$$
$$F_L = F_A - \rho C_p K_z \frac{\partial \theta}{\partial z}. \quad (11)$$

It should be noted that as F_L does not include lateral sources of ocean heat, this parameterization may overestimate the entrainment heat flux if vertical processes do not dominate. The thermal forcing drives an initial ice growth that, through brine rejection and haline convection, results in an entrainment heat flux from the Atlantic Water layer (F_E), with a magnitude given by

$$F_E = F_L \frac{\lambda_{TB}}{(\lambda_{SD} + \lambda_{TB})}. \quad (12)$$

The term λ_{SD} is known as the "salt deficit" and represents the stabilizing freshwater content, relative to the salinity at the base of the halocline, that must be eroded by brine rejection in order to overturn the water column and drive deep convection; λ_{TB} is known as the "thermal barrier" and represents the available heat relative to the freezing point

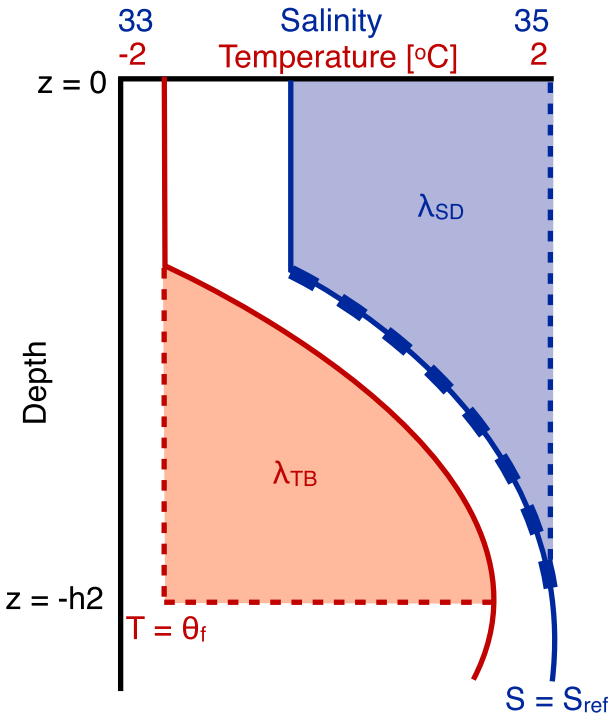

FIG. 10. Schematic showing an idealized temperature and salinity profile in the absence of a cold halocline (i.e., there is no significant salinity gradient over the region of constant near-freezing temperatures), and the regions of the water column that are integrated through Eq. (13) to determine the magnitude of λ_{SD} (blue) and λ_{TB} (red). Variable λ_{SD} represents the stabilizing freshwater content relative to S_{ref} that must be eroded by brine rejection in order to overturn the water column and drive deep convection; λ_{TB} represents the available heat relative to θ_f that can be entrained into the mixed layer from the Atlantic Water layer. The thick dashed blue line represents the region of the water column referred to as the halocline in this parameterization and indicates the depth range over which the average diffusive heat flux is calculated.

that can be entrained into the mixed layer from the Atlantic Water layer (Fig. 10; Martinson and Iannuzzi 1998); and λ_{SD} and λ_{TB} are calculated through vertical integration between the base of the halocline ($z = -h2$; defined as the depth at which the salinity gradient becomes less than $10^{-3}\,\text{m}^{-1}$, see Fig. 10) and the surface ($z = 0$) and are presented in terms of ice thickness (i.e., how much ice would need to form to fully erode the stabilizing freshwater content, and how much ice could be prevented from forming by the heat contained within the Atlantic Water layer):

$$\lambda_{TB} = \int_{z=-h2}^{z=0} (\theta - \theta_f)\frac{\rho C_p}{\rho_I L_I}\,dz,$$
$$\lambda_{SD} = \int_{z=-h2}^{z=0} (S_{ref} - S)\sigma^{-1}\,dz. \qquad (13)$$

Here S_{ref} is the reference salinity at the base of the halocline, and $\sigma^{-1} = 0.03$ is a factor used to convert λ_{SD} into units of ice thickness, based on an ice salinity of 5 PSU (Martinson and Iannuzzi 1998; Vancoppenolle et al. 2009a,b). The thickness of ice that can be prevented from forming by this entrainment heat flux over a 6-month period is given by

$$\Delta h_{\text{Ice}} = \left(\frac{F_E}{\rho_I L_I}\right)\Delta t, \qquad (14)$$

where Δt is 180 days. Applying this parameterization to the final temperature and salinity profiles from each model run in which the cold halocline has been fully eroded shows that the entrainment heat flux can prevent an average of 57 cm of sea ice from forming over 6 months, with a range of 41–64 cm depending on the exact details of the stratification. This is significantly greater than the effect of the elevated diffusive heat flux and represents a 40% reduction in the thickness of sea ice that could have been formed if a cold halocline was present. If Δt is changed to 4 months, the average thickness of ice that can be prevented from forming decreases to 38 cm. The results are similar to those of Linders and Björk (2013), who used a 1D model to show that sea ice growth could be reduced by up to 60 cm over a single year compared to if a cold halocline was present, representing a 22% fractional reduction. The absence of the cold halocline resulted in the formation of a significantly deeper mixed layer, which drove a maximum ocean–ice heat flux of approximately $12\,\text{W}\,\text{m}^{-2}$ at the end of winter (compared to a near-zero ocean–ice heat flux when the cold halocline was present). Furthermore, the study of Steele and Boyd (1998) suggests that, because of the erosion of the cold halocline in the Eurasian Basin during the mid-1990s, the annual average heat flux to the underside of the sea ice increased by 30%–40%.

The thickness of sea ice that can be prevented from forming by this entrainment heat flux is sensitive to the choice of parameters and should not be directly compared to the estimates of equivalent ice loss driven by the elevated diffusive heat flux. However, the difference in the magnitude of the two estimates suggests that the erosion of the cold halocline is the dominant of the two processes.

5. Discussion

Using a simple 1D model of the Arctic Ocean, we have shown that elevated velocity shear in the Eurasian Basin initially causes the mixed layer to warm (first 10–20 years) because of higher diffusivities and an enhanced diffusive heat flux. However, after this initial period, the mixed layer cools across much of the parameter space

because of both the elevated freshwater input and a deepening of the halocline increasing the strength of the stratification and reducing the magnitude of the diffusivity of the Atlantic Water layer. At the same time, the elevated diffusivity can erode the cold halocline within 10 years (i.e., the deepening of the halocline removes the stratification barrier that exists between the mixed layer and the top of the Atlantic Water layer). In this section we discuss the relevance of our results in a wider Arctic context, the time scales over which the different processes that lead to sea ice melt are important, and the effect that the different stratification found in the Canadian Basin has compared to the Eurasian Basin. We finish with a brief discussion of the model limitations.

a. Time scales

Both the elevated diffusive heat flux and the erosion of the cold halocline can affect sea ice thickness in the Eurasian Basin. However, the magnitude of their effects, and the time scales over which they operate, are fundamentally different. For any increase in the shear, the elevated diffusive heat flux very quickly leads to sea ice melting at the surface by driving heat into the mixed layer (Fig. 5). In contrast, it takes time for the elevated mixing to fully erode the cold halocline (Fig. 9) and for the mixed layer to be in direct contact with the Atlantic Water layer. Once the two layers are able to directly interact, a simple parameterization suggests that the heat entrainment driven by haline convection can prevent half a meter of sea ice growth in 6 months. This is significantly greater than the effect of the elevated diffusive heat flux alone, where the maximum increase in mixed layer heat content corresponds to an equivalent net sea ice melt of only 16 cm after 40 years. Therefore, despite the elevated diffusive heat flux dominating initially, it becomes insignificant once the cold halocline, and thus the stratification barrier between the mixed layer and the Atlantic Water layer, has been fully eroded.

b. Canadian Basin

Throughout this paper we have focused on the Eurasian Basin, where constant near-freezing temperatures are found throughout the halocline. In contrast, in the Canadian Basin, a temperature maximum exists in the upper 150 m of the water column because of the inflow of summer Pacific Water (sPW) through Bering Strait (Fig. 11a; Steele et al. 2004; Timmermans et al. 2014). Summer Pacific Water contains enough heat to melt ≈70 cm of sea ice (based on the heat content in the upper 155 m from an annual average profile taken from MIMOC), and thus elevated vertical mixing in the Canadian Basin may not need to penetrate so far into the water column before it can drive a significant heat flux to the surface. At the same time, however, the much stronger stratification in the central Canadian Basin due to the surface convergence of freshwater in the Beaufort Gyre (Proshutinsky et al. 2009) may act to offset the effect of this shallower heat source.

To explore how the markedly different stratification in the Canadian Basin may respond to the competing effects of elevated vertical mixing and increased freshwater input, the model was rerun using initial profiles representative of the central Canadian Basin. The winter temperature and salinity profiles (Fig. 11a) were extracted from MIMOC between 72° and 80°N and 130° and 160°W, and the shear squared profile (Fig. 11c) is based on the average of 37 XCP casts collected during the 1985 Arctic Internal Wave Experiment (D'Asaro and Morehead 1991). Rather than using double exponential curves to smooth the velocity shear profiles as in the Eurasian Basin, the shear profiles were smoothed with a fourth-order Savitzky–Golay filter that removed the sharp gradients but ensured the overall shape was maintained. Consistent with a shallower mixed layer depth (21 m in the control run compared to 31 m in the Eurasian Basin; Peralta-Ferriz and Woodgate 2015), the ocean stress applied at the surface was reduced to $0.02\,\mathrm{N\,m^{-2}}$. Through Eq. (2), the diffusivity profile (Fig. 11d) was matched to the observations of Guthrie et al. (2013) and Lique et al. (2014) by using the same choice of parameters as those used in the Eurasian Basin, except for the value of α, which was increased to 2 to better match the observations below 250 m. The $R^{\theta}(z)$ and $R^{S}(z)$ terms in Eq. (1) were recalculated (dotted lines in Fig. 3) to match the changed θ, S, and diffusivity profiles in the Canadian Basin. Furthermore, the depths of ZMax were changed to 155 m (the core of winter Pacific Water; Steele et al. 2004), 410 m (the core of the Atlantic Water layer), and 282 m (midway between the core of the winter Pacific Water and the core of the Atlantic Water layer).

As in the Eurasian Basin, the mixed layer temperature increases in all model runs in which the shear is elevated (Fig. 12). The magnitude of the warming depends strongly on the strength of the shear (as higher diffusivities drive a larger diffusive heat flux), but is significantly less sensitive to the depth to which it penetrates. Indeed, when ZMax is 410 m, the maximum increase in the mixed layer temperature after 40 years is 0.11°C, reducing only slightly to 0.10° and 0.09°C when ZMax is 282 and 155 m, respectively. This lack of dependence on ZMax is due to the much stronger stratification found in the Canadian Basin than in the Eurasian Basin (cf. Fig. 11b with Fig. 2b). Even when the elevated velocity

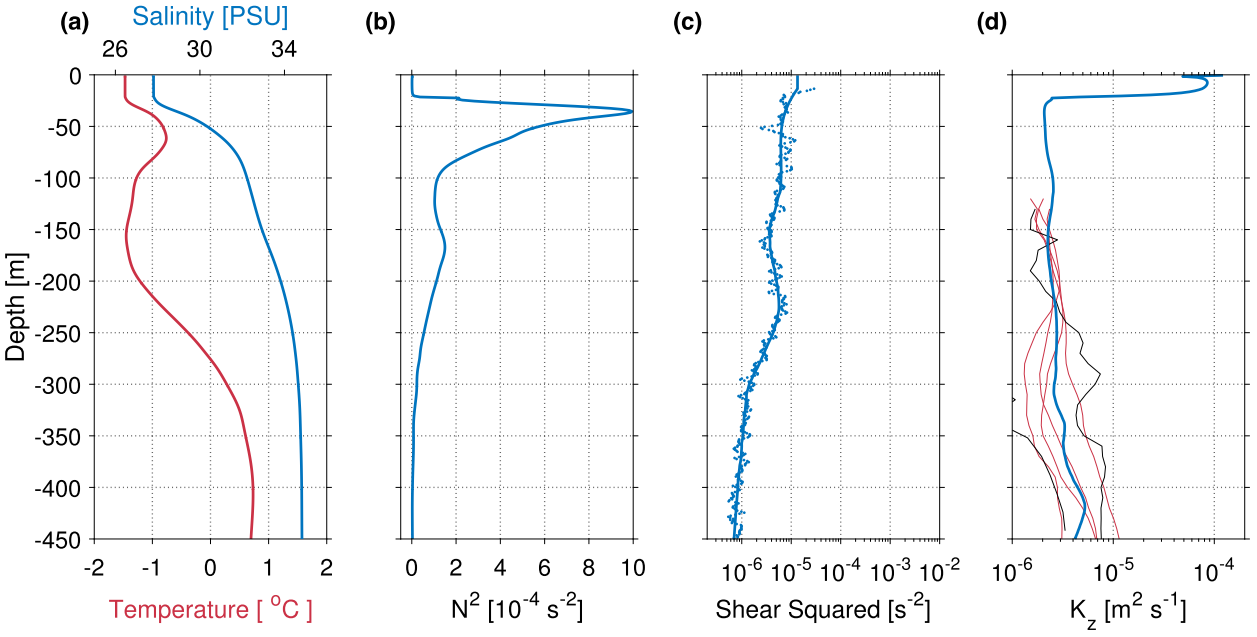

FIG. 11. Initial profiles of (a) temperature and salinity averaged over the central Canadian Basin from MIMOC; (b) the corresponding buoyancy frequency; (c) the climatological shear squared, derived from XCP data collected during the 1985 Arctic Internal Wave Experiment; and (d) the corresponding vertical diffusivity due to shear instability associated with internal wave breaking (blue line), parameterized through Eq. (2). The thin black lines in (d) show the vertical diffusivity in the Canadian Basin estimated by Guthrie et al. (2013), and the red lines show the vertical diffusivity profiles parameterized from profiling moorings deployed in the Canadian Basin from Lique et al. (2014). Note the different range on the salinity axis compared to Fig. 2.

shear extends to the depth of the Atlantic Water layer for 6 months of each year, the overall increase in the diffusivity is sufficiently small (the diffusivity does not exceed $10^{-5}\,\mathrm{m^2\,s^{-1}}$ anywhere in the water column) that there is effectively no change in the diffusive heat flux from the Atlantic Water layer. Consequently, the only heat available to be fluxed into the mixed layer is that contained in the sPW, which is accessible to even the shallowest increases in diffusivity. As a result, shallower mixing in the Canadian Basin can transfer significantly more heat into the mixed layer than in the Eurasian Basin (cf. Figs. 12a, b with Figs. 5a,b), but the opposite is true for deeper mixing as it cannot release the heat held within the Atlantic Water layer. Furthermore, Fig. 12 shows that the positive trend in the mixed layer temperature does not reverse like in the Eurasian Basin, as the stratification does not strengthen over the Atlantic Water layer. Instead, a pseudo-steady state is reached where the flux of heat into the mixed layer during ice-free periods is removed by the $R^{\theta}(z)$ term during ice covered periods, as evident from the seasonal cycle in Fig. 12.

Despite the increase in mixed layer temperature from the control run, Fig. 13 shows that after 40 years (blue line in Fig. 12) the parameter space is dominated by net sea ice formation. The ice melt contours lie perpendicular to the change in mixed layer temperature contours, indicating that freshening of the mixed layer and the corresponding increase in the local freezing point is outcompeting the increase in mixed layer temperature. The maximum equivalent net sea ice growth is 6 cm. Sea ice melt is restricted to regions of parameter space with strongly elevated shear and little or no increase in the freshwater input. The maximum equivalent net sea ice melt is only 5 cm (compared to 16 cm in the Eurasian Basin) because of the cooler and shallower mixed layer in the Canadian Basin.

In contrast to the Eurasian Basin, a visual examination of the θ and S profiles suggests that the Canadian Basin halocline remains stable throughout the parameter space, and therefore, as the stratification barrier is never eroded, the heat contained within the Atlantic Water layer can never be directly entrained into the mixed layer. On the other hand, as the sPW lies directly beneath the mixed layer, weakening of the stratification over the sPW may allow the heat in this region to be entrained into the mixed layer. However, if the parameterization discussed in section 4b is applied to all Canadian Basin model runs after 40 years, the reduction in sea ice formation due to haline convection and heat entrainment from the sPW is tiny.

It is also interesting to note that as the heat in the Arctic's Atlantic Water layer is advective in origin,

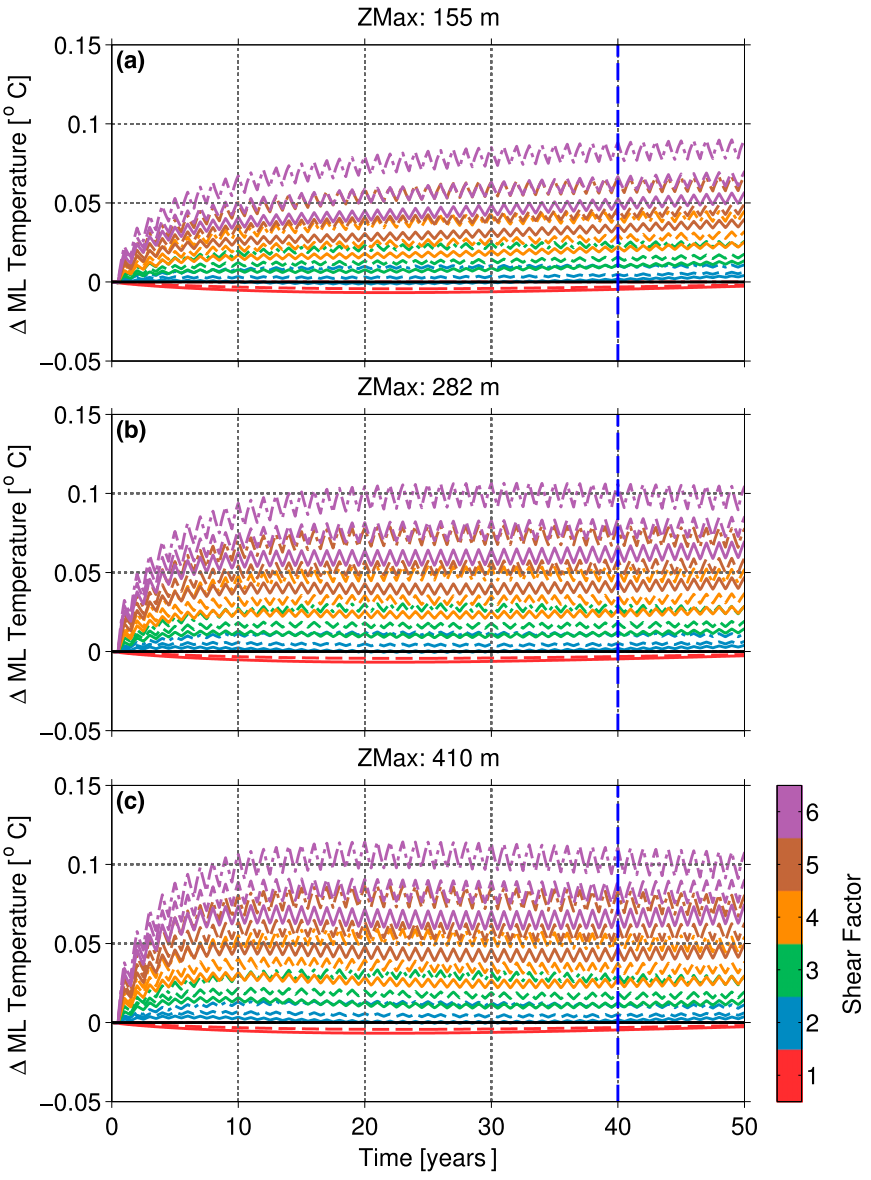

FIG. 12. Time series of the deviation in the mixed layer temperature from the control value in the Canadian Basin for model runs in which the velocity shear profiles have been perturbed for 6 months of each year, down to a ZMax of (a) 155, (b) 282, and (c) 410 m. The color of each line represents the shear factor, and the solid, dashed, and dot–dashed lines represent a 30%, 15%, and 0% increase in the freshwater input, respectively.

changes in the strength of the vertical mixing and the temperature of the Atlantic Water layer upstream in the Eurasian Basin may play an important role in determining the importance of the Atlantic Water layer in the Canadian Basin. On the one hand, if elevated mixing releases more heat to the upper layers of the Eurasian Basin and thus the Atlantic Water layer becomes cooler downstream in the Canadian Basin, it will become even less important for the ongoing melting of sea ice at the surface. In contrast, if the opposite occurs and the Atlantic Water layer becomes warmer as less heat is released in the Eurasian Basin, the heat contained within the Atlantic Water layer may play a more important role.

c. *Relevance for future sea ice melt*

As upper bound estimates, our results show that an elevated diffusive heat flux could increase the mixed layer heat content sufficiently after 40 years to melt an equivalent of 5 cm of sea ice in the Canadian Basin and

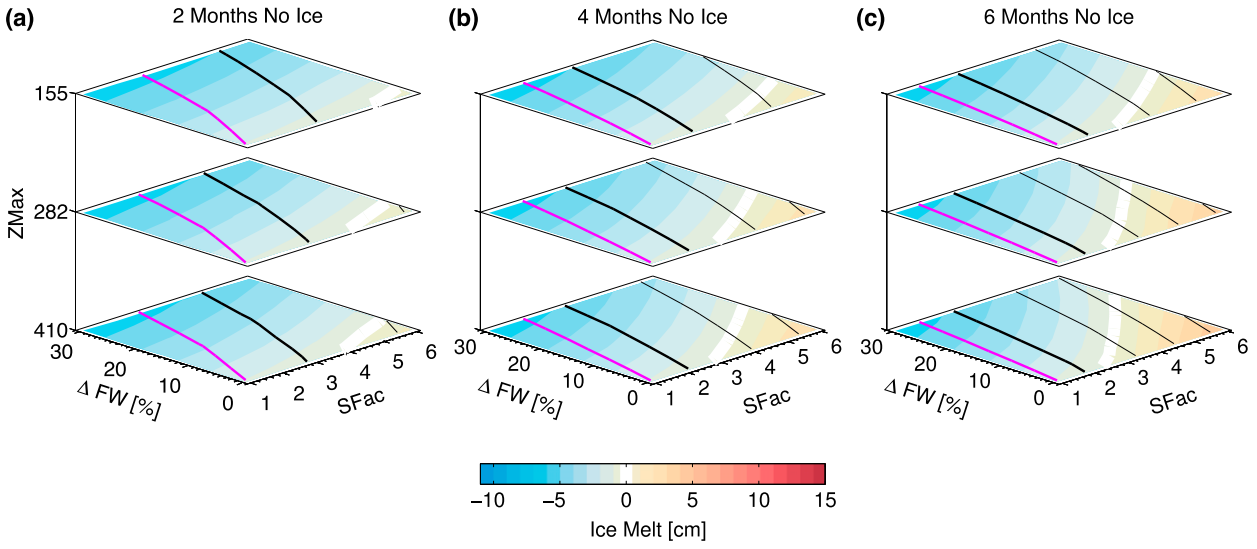

FIG. 13. Thickness of ice (color contours) that could be melted/formed because of the change in mixed layer heat content after 40 years of each model run in the Canadian Basin, plotted in the same format as Fig. 8. Negative ice melt indicates ice formation. Overlain are contours showing the deviation in the mixed layer temperature from the control run. Solid contours indicate an increase in the mixed layer temperature, and dashed contours indicate a decrease in the mixed layer temperature. The contour interval is 0.03°C, with the zero contour marked in magenta and the first contour (i.e., ±0.03°C) marked in bold.

4 cm of sea ice in the Eurasian Basin before the cold halocline has been fully eroded. Once the cold halocline has been fully eroded, a simple parameterization of the entrainment heat flux driven by haline convection suggests it could melt half a meter of sea ice in 6 months. How relevant are these processes compared to the other mechanisms responsible for sea ice melt within the Arctic?

The near-surface temperature maximum (NSTM) has recently become a persistent feature of the Canadian Basin water column because of the decline in summer sea ice extent (Jackson et al. 2010, 2011). This decrease in sea ice extent has caused the amount of solar radiation absorbed into the upper ocean to increase from 200 to 400 MJ m^{-2} yr^{-1} between 1979–92 and 1992–2005 (Perovich et al. 2007), warming the mixed layer. Using a numerical model, Steele et al. (2011) showed that the heat content of the NSTM in autumn is sufficient to melt 1 m of sea ice over the following winter, and although some of this heat will be lost directly to the atmosphere, the remainder will reduce sea ice growth. Furthermore, Steele et al. (2008) show that between 1965 and 1995, the increase in the upper-ocean temperature during summer in the southern Chukchi and western Beaufort Seas (driven by a positive trend in the Arctic Oscillation) was sufficient to reduce winter ice growth by 56–75 cm, and Pinker et al. (2014) suggest that over the entire Arctic, the anomalous solar heating of the ocean in 2007 (120 MJ m^{-2} increase over the 1984–2009 mean) could decrease winter ice growth by 44 cm. All these estimates are significantly greater than the effect of the elevated diffusive heat flux in both the Eurasian and Canadian basins, but are comparable to the effect of the entrainment heat flux driven by sea ice formation in the absence of a cold halocline.

Our results therefore suggest that the erosion of the cold halocline represents the most important process considered here for the ongoing melting of Arctic sea ice, and an elevated diffusive heat flux driven by periodic increases in vertical mixing will play only a very limited role. It will take at least a decade for the cold halocline to be eroded in the Eurasian Basin (while it is never eroded in the Canadian Basin), and in the meantime, our results suggest that elevated vertical mixing will not result in a significant loss of sea ice at the surface.

d. Model limitations

As discussed earlier, there are a number of processes that are not resolved in our 1D model that may also play a role in determining how Arctic sea ice and stratification will respond to the competing effects of elevated vertical mixing and enhanced freshwater input. For example, the effects of ice–ocean interactions (e.g., brine rejection) are likely to act in opposition to any melt/formation of sea ice driven by elevated vertical mixing. As excess heat is brought up to the surface by either a diffusive or entrainment heat flux (once the cold halocline has been fully eroded), sea ice melt will release freshwater, stabilizing the water column and limiting the extent to which heat can continue to be brought to the

surface. Conversely, sea ice formation will release brine, weakening the stratification and allowing more heat to be brought to the surface.

In addition, as the magnitudes of $R^{\theta}(z)$ and $R^{S}(z)$ are fixed at that required to balance the effect of mixing in the control run, we have not been able to consider the effect that any interplay between elevated vertical mixing and seasonal and long-term changes in the processes that set the stratification of the Arctic Ocean may have on the flux of heat to the underside of the sea ice. In the real Arctic, however, the processes that set the stratification will undoubtedly change on the time scales we consider, and despite our current knowledge of these changes being poorly constrained, they may have important implications for our results. For example, on seasonal time scales, a negative surface heat flux and brine rejection from sea ice formation at the end of summer will act to deepen the mixed layer, entraining water from the pycnocline and thinning the cold halocline. While this process may not deepen the mixed layer sufficiently such that it entrains water that is above the freezing point (unlike when the cold halocline is absent), a seasonal thinning of the cold halocline and the weaker salinity stratification may allow the enhanced vertical mixing to flux more heat into the mixed layer. On longer time scales, Davis et al. (2014) suggest that over the coming decades, the possible change in momentum input at the ocean surface, linked with the change in sea ice conditions, might affect the rate of freshwater accumulation in the Beaufort Gyre and drive a long-term positive trend in the stability of the water column. At the same time, Lique et al. (2015) show that strengthening of the Beaufort Gyre can strongly affect the circulation of the Atlantic Water boundary current and limit the penetration of heat into the Canadian Basin. These and other seasonal (e.g., the absorption of solar radiation during the ice-free summer) and long-term Arctic changes (e.g., variability in the mechanisms that form the cold halocline) will likely have significant impacts on the stratification throughout the water column and the temperature of the Atlantic Water layer, but we defer the investigation of these impacts to future studies.

6. Conclusions

The aim of this study was to investigate how the competing effects of elevated vertical mixing and enhanced freshwater input at the surface may affect the stratification, the stability of the cold halocline, and the sea ice cover at the surface over the coming decades. Using a 1D model in which the diffusivity is assumed to be a function of the shear instability associated with internal wave breaking, we perturbed the strength of the velocity shear, the depth to which this elevated shear penetrates, the length of the ice-free season, and the freshwater input at the surface through a wide parameter space that is applicable for a future Arctic.

In the Eurasian Basin, elevated shear drives an initial increase in mixed layer temperature due to an enhanced diffusive heat flux at the base of the mixed layer. The magnitude of the diffusive heat flux depends predominantly on the depth to which the elevated shear penetrates, as deeper mixing is able to interact with the strong Atlantic Water layer temperature gradient. Most importantly, however, after about a decade, the elevated freshwater input, a deeper halocline, and the associated increase in the strength of the stratification over the Atlantic Water layer begins to dominate, and the mixed layer begins to cool as the corresponding decrease in the diffusivity reduces the supply of heat to the surface. After 40 years, the maximum increase in the mixed layer heat content driven by the elevated diffusive heat flux is equivalent to $\approx$16 cm of sea ice melt. In other parts of parameter space, the elevated freshwater input, increased local freezing point, stronger stratification, and weaker vertical heat flux results in an equivalent net formation of $\approx$11 cm of sea ice.

The stability of the cold halocline in the Eurasian Basin is strongly affected by the elevated shear and, when it penetrates into the Atlantic Water layer, the cold halocline can be fully eroded within 10 years. Once the stratification barrier associated with the cold halocline has been fully eroded, the heat contained within the Atlantic Water layer can be directly entrained into the mixed layer, and a simple parameterization suggests that a buoyancy-driven heat entrainment feedback could prevent half a meter of sea ice forming over 6 months.

In the Canadian Basin, the much stronger stratification outcompetes the elevated velocity shear, and the increase in the diffusivity is small. There is little increase in the diffusive heat flux from the Atlantic Water layer and, despite the heat contained within the shallower sPW, the parameter space is dominated by sea ice formation due to freshwater input at the surface (the maximum equivalent sea ice melt is only 5 cm). Because of the limited change in diffusivity, the halocline is never fully eroded in the Canadian Basin.

Comparing the results to other major processes responsible for sea ice melt in the Arctic suggests that the quantity of ice that can be melted by the elevated diffusive heat flux in both the Eurasian and Canadian basins is insignificant, and instead it is the erosion of the cold halocline that represents the largest risk for ongoing melting of Arctic sea ice. Therefore, until, or indeed unless, the cold halocline is eroded, our results suggest that the sea ice cover in the Arctic will remain largely

immune to the heat contained within the Atlantic Water layer, and the role of the ocean will be limited to the part it plays in the ice–albedo feedback effect and the bottom melting of sea ice through the absorption of solar radiation.

Acknowledgments. We thank Ilker Fer for providing access to the microstructure observations in Fig. 2 and two anonymous reviewers for their very helpful and constructive feedback. This study has been funded by the UK Natural Environment Research Council (NERC) and NSF Grants ARC-1135072 and ARC-0909408. All model data used in this study are available by contacting the corresponding author by email (petvis@bas.ac.uk).

REFERENCES

Aagaard, K., L. K. Coachman, and E. Carmack, 1981: On the halocline of the Arctic Ocean. *Deep-Sea Res.*, **28A**, 529–545, doi:10.1016/0198-0149(81)90115-1.

Ardyna, M., M. Babin, M. Gosselin, E. Devred, L. Rainville, and J. Tremblay, 2014: Recent Arctic Ocean sea-ice loss triggers novel fall phytoplankton blooms. *Geophys. Res. Lett.*, **41**, 6207–6212, doi:10.1002/2014GL061047.

Barthélemy, A., T. Fichefet, H. Goosse, and G. Madec, 2015: Modeling the interplay between sea ice formation and the oceanic mixed layer: Limitations of simple brine rejection parameterizations. *Ocean Modell.*, **86**, 141–152, doi:10.1016/j.ocemod.2014.12.009.

Bintanja, R., and F. M. Selten, 2014: Future increases in Arctic precipitation linked to local evaporation and sea-ice retreat. *Nature*, **509**, 479–482, doi:10.1038/nature13259.

Bjork, G., 1989: A one-dimensional time-dependent model for the vertical stratification of the upper Arctic Ocean. *J. Phys. Oceanogr.*, **19**, 52–76, doi:10.1175/1520-0485(1989)019<0052:AODTDM>2.0.CO;2.

Bourgain, P., and J. C. Gascard, 2011: The Arctic Ocean halocline and its interannual variability from 1997 to 2008. *Deep-Sea Res. I*, **58**, 745–756, doi:10.1016/j.dsr.2011.05.001.

Burchard, H., K. Bolding, and M. R. Villarreal, 1999: GOTM, a general ocean turbulence model: Theory, implementation and test cases. Tech. Rep. EUR 18745, European Commission, 103 pp.

D'Asaro, E. A., and M. D. Morehead, 1991: Internal waves and velocity fine structure in the Arctic Ocean. *J. Geophys. Res.*, **96**, 12 725–12 738, doi:10.1029/91JC01071.

——, and J. H. Morison, 1992: Internal waves and mixing in the Arctic Ocean. *Deep-Sea Res.*, **39A**, S459–S484, doi:10.1016/S0198-0149(06)80016-6.

Davis, P. E. D., C. Lique, and H. L. Johnson, 2014: On the link between Arctic sea ice decline and the freshwater content of the Beaufort Gyre: Insights from a simple process model. *J. Climate*, **27**, 8170–8184, doi:10.1175/JCLI-D-14-00090.1.

Dosser, H. V., L. Rainville, and J. M. Toole, 2014: Near-inertial internal wave field in the Canada basin from ice-tethered profilers. *J. Phys. Oceanogr.*, **44**, 413–426, doi:10.1175/JPO-D-13-0117.1.

Fer, I., 2009: Weak vertical diffusion allows maintenance of cold halocline in the central Arctic. *Atmos. Oceanic Sci. Lett.*, **2**, 148–152, doi:10.1080/16742834.2009.11446789.

——, 2014: Near-inertial mixing in the central Arctic Ocean. *J. Phys. Oceanogr.*, **44**, 2031–2049, doi:10.1175/JPO-D-13-0133.1.

Garrett, C., and W. Munk, 1975: Space-time scales of internal waves: A progress report. *J. Geophys. Res.*, **80**, 291–297, doi:10.1029/JC080i003p00291.

Guthrie, J. D., J. H. Morison, and I. Fer, 2013: Revisiting internal waves and mixing in the Arctic Ocean. *J. Geophys. Res. Oceans*, **118**, 3966–3977, doi:10.1002/jgrc.20294.

Haine, T. W. N., and Coauthors, 2015: Arctic freshwater export: Status, mechanisms, and prospects. *Global Planet. Change*, **125**, 13–35, doi:10.1016/j.gloplacha.2014.11.013.

Halle, C., and R. Pinkel, 2003: Internal wave variability in the Beaufort Sea during the winter of 1993/1994. *J. Geophys. Res.*, **108**, 3210, doi:10.1029/2000JC000703.

Jackson, J. M., E. C. Carmack, F. A. McLaughlin, S. E. Allen, and R. G. Ingram, 2010: Identification, characterization, and change of the near-surface temperature maximum in the Canada Basin, 1993–2008. *J. Geophys. Res.*, **115**, C05021, doi:10.1029/2009JC005265.

——, S. E. Allen, F. A. McLaughlin, R. A. Woodgate, and E. C. Carmack, 2011: Changes to the near-surface waters in the Canada Basin, Arctic Ocean from 1993–2009: A basin in transition. *J. Geophys. Res.*, **116**, C10008, doi:10.1029/2011JC007069.

Kawaguchi, Y., S. Nishino, and J. Inoue, 2015: Fixed-point observation of mixed layer evolution in the seasonally ice-free Chukchi Sea: Turbulent mixing due to gale winds and internal gravity waves. *J. Phys. Oceanogr.*, **45**, 836–853, doi:10.1175/JPO-D-14-0149.1.

Killworth, P. D., and J. M. Smith, 1984: A one-and-a-half dimensional model for the Arctic halocline. *Deep-Sea Res.*, **31A**, 271–293, doi:10.1016/0198-0149(84)90105-5.

Large, W. G., J. C. Mcwilliams, and S. C. Doney, 1994: Oceanic vertical mixing: A review and a model with a nonlocal boundary layer parameterization. *Rev. Geophys.*, **32**, 363–403, doi:10.1029/94RG01872.

Levine, M. D., C. A. Paulson, and J. H. Morison, 1985: Internal waves in the Arctic Ocean: Comparisons with lower-latitude observations. *J. Phys. Oceanogr.*, **15**, 800–809, doi:10.1175/1520-0485(1985)015<0800:IWITAO>2.0.CO;2.

——, ——, and ——, 1987: Observations of internal gravity waves under the Arctic pack ice. *J. Geophys. Res.*, **92**, 779–782, doi:10.1029/JC092iC01p00779.

Linders, J., and G. Björk, 2013: The melt-freeze cycle of the Arctic Ocean ice cover and its dependence on ocean stratification. *J. Geophys. Res. Oceans*, **118**, 5963–5976, doi:10.1002/jgrc.20409.

Lique, C., and M. Steele, 2012: Where can we find a seasonal cycle of the Atlantic water temperature within the Arctic Basin? *J. Geophys. Res.*, **117**, C03026, doi:10.1029/2011JC007612.

——, J. D. Guthrie, M. Steele, A. Proshutinsky, J. H. Morison, and R. Krishfield, 2014: Diffusive vertical heat flux in the Canada Basin of the Arctic Ocean inferred from moored instruments. *J. Geophys. Res. Oceans*, **119**, 496–508, doi:10.1002/2013JC009346.

——, H. L. Johnson, and P. E. D. Davis, 2015: On the interplay between the circulation in the surface and the intermediate layers of the Arctic Ocean. *J. Phys. Oceanogr.*, **45**, 1393–1409, doi:10.1175/JPO-D-14-0183.1.

Markus, T., J. C. Stroeve, and J. Miller, 2009: Recent changes in Arctic sea ice melt onset, freezeup, and melt season length. *J. Geophys. Res.*, **114**, C12024, doi:10.1029/2009JC005436.

Martin, T., M. Steele, and J. Zhang, 2014: Seasonality and long-term trend of Arctic Ocean surface stress in a model. *J. Geophys. Res.*, **119**, 1723–1738, doi:10.1002/2013JC009425.

Martinson, D. G., 1990: Evolution of the southern ocean winter mixed layer and sea ice: Open ocean deepwater formation and ventilation. *J. Geophys. Res.*, **95**, 11 641–11 654, doi:10.1029/JC095iC07p11641.

——, and R. A. Iannuzzi, 1998: Antarctic Ocean-ice interactions: Implications from ocean bulk property distributions in the Weddell Gyre. *Antarctic Sea Ice: Physical Processes, Interactions and Variability*, M. O. Jeffries, Ed., Antarctic Research Series, Vol. 74, Amer. Geophys. Union, 243–271.

——, and M. Steele, 2001: Future of the Arctic sea ice cover: Implications of an Antarctic analog. *Geophys. Res. Lett.*, **28**, 307–310, doi:10.1029/2000GL011549.

Maykut, G. A., and N. Untersteiner, 1971: Some results from a time-dependent thermodynamic model of sea ice. *J. Geophys. Res.*, **76**, 1550–1575, doi:10.1029/JC076i006p01550.

Morison, J. H., C. E. Long, and M. D. Levine, 1985: Internal wave dissipation under sea ice. *J. Geophys. Res.*, **90**, 11 959–11 966, doi:10.1029/JC090iC06p11959.

Munk, W. H., 1966: Abyssal recipes. *Deep-Sea Res. Oceanogr. Abstr.*, **13**, 707–730, doi:10.1016/0011-7471(66)90602-4.

——, and C. Wunsch, 1998: Abyssal recipes II: energetics of tidal and wind mixing. *Deep-Sea Res. I*, **45**, 1977–2010, doi:10.1016/S0967-0637(98)00070-3.

Nishino, S., Y. Kawaguchi, J. Inoue, T. Hirawake, A. Fujiwara, R. Futsuki, J. Onodera, and M. Aoyama, 2015: Nutrient supply and biological response to wind-induced mixing, inertial motion, internal waves, and currents in the northern Chukchi Sea. *J. Geophys. Res. Oceans*, **120**, 1975–1992, doi:10.1002/2014JC010407.

Nummelin, A., C. Li, and L. H. Smedsrud, 2015: Response of Arctic Ocean stratification to changing river runoff in a column model. *J. Geophys. Res. Oceans*, **120**, 2655–2675, doi:10.1002/2014JC010571.

Overland, J. E., and M. Wang, 2013: When will the summer Arctic be nearly sea ice free? *Geophys. Res. Lett.*, **40**, 2097–2101, doi:10.1002/grl.50316.

——, J. M. Adams, and N. A. Bond, 1997: Regional variation of winter temperatures in the Arctic. *J. Climate*, **10**, 821–837, doi:10.1175/1520-0442(1997)010<0821:RVOWTI>2.0.CO;2.

Pacanowski, R. C., and G. H. Philander, 1981: Parameterization of vertical mixing in numerical models of tropical oceans. *J. Phys. Oceanogr.*, **11**, 1443–1451, doi:10.1175/1520-0485(1981)011<1443:POVMIN>2.0.CO;2.

Peralta-Ferriz, C., and R. A. Woodgate, 2015: Seasonal and interannual variability of pan-Arctic surface mixed layer properties from 1979 to 2012 from hydrographic data, and the dominance of stratification for multiyear mixed layer depth shoaling. *Prog. Oceanogr.*, **134**, 19–53, doi:10.1016/j.pocean.2014.12.005.

Perovich, D. K., B. Light, H. Eicken, K. F. Jones, K. Runciman, and S. V. Nghiem, 2007: Increasing solar heating of the Arctic Ocean and adjacent seas, 1979–2005: Attribution and role in the ice-albedo feedback. *Geophys. Res. Lett.*, **34**, L19505, doi:10.1029/2007GL031480.

——, J. A. Richter-Menge, K. F. Jones, and B. Light, 2008: Sunlight, water, and ice: Extreme Arctic sea ice melt during the summer of 2007. *Geophys. Res. Lett.*, **35**, L11501, doi:10.1029/2008GL034007.

Peterson, B. J., R. M. Holmes, J. W. McClelland, C. J. Vörösmarty, R. B. Lammers, A. I. Shiklomanov, I. A. Shiklomanov, and S. Rahmstorf, 2002: Increasing river discharge to the Arctic Ocean. *Science*, **298**, 2171–2173, doi:10.1126/science.1077445.

Pinkel, R., 2005: Near-inertial wave propagation in the western Arctic. *J. Phys. Oceanogr.*, **35**, 645–665, doi:10.1175/JPO2715.1.

Pinker, R. T., X. Niu, and Y. Ma, 2014: Solar heating of the Arctic Ocean in the context of ice-albedo feedback. *J. Geophys. Res.*, **119**, 8395–8409, doi:10.1002/2014JC010232.

Plueddemann, A. J., 1992: Internal wave observations from the Arctic environmental drifting buoy. *J. Geophys. Res.*, **97**, 12 619–12 638, doi:10.1029/92JC01098.

Polyakov, I. V., J. E. Walsh, and R. Kwok, 2012: Recent changes of Arctic multiyear sea ice coverage and the likely causes. *Bull. Amer. Meteor. Soc.*, **93**, 145–151, doi:10.1175/BAMS-D-11-00070.1.

Proshutinsky, A., and Coauthors, 2009: Beaufort Gyre freshwater reservoir: State and variability from observations. *J. Geophys. Res.*, **114**, C00A10, doi:10.1029/2008JC005104.

Rabe, B., and Coauthors, 2011: An assessment of Arctic Ocean freshwater content changes from the 1990s to the 2006–2008 period. *Deep-Sea Res. I*, **58**, 173–185, doi:10.1016/j.dsr.2010.12.002.

Rainville, L., and P. Winsor, 2008: Mixing across the Arctic Ocean: Microstructure observations during the Beringia 2005 Expedition. *Geophys. Res. Lett.*, **35**, L08606, doi:10.1029/2008GL033532.

——, and R. A. Woodgate, 2009: Observations of internal wave generation in the seasonally ice-free Arctic. *Geophys. Res. Lett.*, **36**, L23604, doi:10.1029/2009GL041291.

——, C. M. Lee, and R. A. Woodgate, 2011: Impact of wind-driven mixing in the Arctic Ocean. *Oceanography*, **24**, 136–145, doi:10.5670/oceanog.2011.65.

Rippeth, T. P., B. J. Lincoln, Y.-D. Lenn, J. A. M. Green, A. Sundfjord, and S. Bacon, 2015: Tide-mediated warming of Arctic halocline by Atlantic heat fluxes over rough topography. *Nat. Geosci.*, **8**, 191–194, doi:10.1038/ngeo2350.

Rudels, B., L. G. Anderson, and E. P. Jones, 1996: Formation and evolution of the surface mixed layer and halocline of the Arctic Ocean. *J. Geophys. Res.*, **101**, 8807–8821, doi:10.1029/96JC00143.

Schmidtko, S., G. C. Johnson, and J. M. Lyman, 2013: MIMOC: A global monthly isopycnal upper-ocean climatology with mixed layers. *J. Geophys. Res. Oceans*, **118**, 1658–1672, doi:10.1002/jgrc.20122.

Shaw, W. J., and T. P. Stanton, 2014: Vertical diffusivity of the western Arctic Ocean halocline. *J. Geophys. Res. Oceans*, **119**, 5017–5038, doi:10.1002/2013JC009598.

Simmons, H. L., R. W. Hallberg, and B. K. Arbic, 2004: Internal wave generation in a global baroclinic tide model. *Deep-Sea Res. II*, **51**, 3043–3068, doi:10.1016/j.dsr2.2004.09.015.

Simpson, J. H., and D. Bowers, 1981: Models of stratification and frontal movement in shelf seas. *Deep-Sea Res.*, **28A**, 727–738, doi:10.1016/0198-0149(81)90132-1.

Sirevaag, A., and I. Fer, 2012: Vertical heat transfer in the Arctic Ocean: The role of double-diffusive mixing. *J. Geophys. Res.*, **117**, C07010, doi:10.1029/2012JC007910.

Steele, M., and T. Boyd, 1998: Retreat of the cold halocline layer in the Arctic Ocean. *J. Geophys. Res.*, **103**, 10 419–10 435, doi:10.1029/98JC00580.

——, J. Morison, W. Ermold, I. Rigor, M. Ortmeyer, and K. Shimada, 2004: Circulation of summer Pacific halocline water in the Arctic Ocean. *J. Geophys. Res.*, **109**, C02027, doi:10.1029/2003JC002009.

——, W. Ermold, and J. Zhang, 2008: Arctic Ocean surface warming trends over the past 100 years. *Geophys. Res. Lett.*, **35**, L02614, doi:10.1029/2007GL031651.

——, ——, and ——, 2011: Modeling the formation and fate of the near-surface temperature maximum in the Canadian Basin of the Arctic Ocean. *J. Geophys. Res.*, **116**, C11015, doi:10.1029/2010JC006803.

Timmermans, M.-L., 2015: The impact of stored solar heat on Arctic sea ice growth. *Geophys. Res. Lett.*, **42**, 6399–6406, doi:10.1002/2015GL064541.

——, J. Toole, R. Krishfield, and P. Winsor, 2008: Ice-tethered profiler observations of the double-diffusive staircase in the Canada Basin thermocline. *J. Geophys. Res.*, **113**, C00A02, doi:10.1029/2008JC004829.

——, and Coauthors, 2014: Mechanisms of Pacific Summer Water variability in the Arctic's central Canada Basin. *J. Geophys. Res. Oceans*, **119**, 7523–7548, doi:10.1002/2014JC010273.

Toole, J. M., M.-L. Timmermans, D. K. Perovich, R. A. Krishfield, A. Proshutinsky, and J. A. Richter-Menge, 2010: Influences of the ocean surface mixed layer and thermohaline stratification on Arctic Sea ice in the central Canada Basin. *J. Geophys. Res.*, **115**, C10018, doi:10.1029/2009JC005660.

Tsamados, M., D. L. Feltham, D. Schroeder, D. Flocco, S. L. Farrell, N. Kurtz, S. W. Laxon, and S. Bacon, 2014: Impact of variable atmospheric and oceanic form drag on simulations of Arctic sea ice. *J. Phys. Oceanogr.*, **44**, 1329–1353, doi:10.1175/JPO-D-13-0215.1.

Turner, J. S., 2010: The melting of ice in the Arctic Ocean: The influence of double-diffusive transport of heat from below. *J. Phys. Oceanogr.*, **40**, 249–256, doi:10.1175/2009JPO4279.1.

Vancoppenolle, M., T. Fichefet, H. Goosse, S. Bouillon, G. Madec, and M. A. M. Maqueda, 2009a: Simulating the mass balance and salinity of Arctic and Antarctic sea ice. 1. Model description and validation. *Ocean Modell.*, **27**, 33–53, doi:10.1016/j.ocemod.2008.10.005.

——, ——, and ——, 2009b: Simulating the mass balance and salinity of Arctic and Antarctic sea ice. 2. Importance of sea ice salinity variations. *Ocean Modell.*, **27**, 54–69, doi:10.1016/j.ocemod.2008.11.003.

Vavrus, S. J., M. M. Holland, A. Jahn, D. A. Bailey, and B. A. Blazey, 2012: Twenty-first-century Arctic climate change in CCSM4. *J. Climate*, **25**, 2696–2710, doi:10.1175/JCLI-D-11-00220.1.

Wang, M., and J. E. Overland, 2009: A sea ice free summer Arctic within 30 years? *Geophys. Res. Lett.*, **36**, L07502, doi:10.1029/2009GL037820.

——, and ——, 2015: Projected future duration of the sea-ice-free season in the Alaskan Arctic. *Prog. Oceanogr.*, **136**, 50–59, doi:10.1016/j.pocean.2015.01.001.